AEDC-TR-75-2

REAL GAS SCALE EFFECTS ON HYPERSONIC LAMINAR BOUNDARY-LAYER PARAMETERS INCLUDING EFFECTS OF ENTROPY-LAYER SWALLOWING

VON KÁRMÁN GAS DYNAMICS FACILITY
ARNOLD ENGINEERING DEVELOPMENT CENTER
AIR FORCE SYSTEMS COMMAND
ARNOLD AIR FORCE STATION, TENNESSEE 37389

December 1975

Final Report for Period March 21 – October 20, 1974

Approved for public release; distribution unlimited.

Prepared for

NATIONAL AERONAUTICS AND SPACE ADMINISTRATION (JSC)
JOHNSON SPACE CENTER
HOUSTON, TEXAS 77058

NOTICES

When U. S. Government drawings specifications, or other data are used for any purpose other than a definitely related Government procurement operation, the Government thereby incurs no responsibility nor any obligation whatsoever, and the fact that the Government may have formulated, furnished, or in any way supplied the said drawings, specifications, or other data, is not to be regarded by implication or otherwise, or in any manner licensing the holder or any other person or corporation, or conveying any rights or permission to manufacture, use, or sell any patented invention that may in any way be related thereto.

Qualified users may obtain copies of this report from the Defense Documentation Center.

References to named commercial products in this report are not to be considered in any sense as an endorsement of the product by the United States Air Force or the Government.

This report has been reviewed by the Information Office (OI) and is releasable to the National Technical Information Service (NTIS). At NTIS, it will be available to the general public, including foreign nations.

APPROVAL STATEMENT

This technical report has been reviewed and is approved for publication.

FOR THE COMMANDER

JIMMY W. MULLINS
Lt Colonel, USAF
Chief Air Force Test Director, VKF
Directorate of Test

FRANK J. PASSARELLO
Colonel, USAF
Director of Test

REPORT DOCUMENTATION PAGE		READ INSTRUCTIONS BEFORE COMPLETING FORM
1. REPORT NUMBER AEDC-TR-75-2	2. GOVT ACCESSION NO.	3. RECIPIENT'S CATALOG NUMBER
4. TITLE *(and Subtitle)* REAL GAS SCALE EFFECTS ON HYPERSONIC LAMINAR BOUNDARY-LAYER PARAMETERS INCLUDING EFFECTS OF ENTROPY-LAYER SWALLOWING		5. TYPE OF REPORT & PERIOD COVERED Final Report, Mar 21 - Oct 20, 1974 6. PERFORMING ORG. REPORT NUMBER
7. AUTHOR(s) J. C. Adams, Jr., W. R. Martindale, A. W. Mayne, Jr., and E. O. Marchand, ARO, Inc.		8. CONTRACT OR GRANT NUMBER(s)
9. PERFORMING ORGANIZATION NAME AND ADDRESS Arnold Engineering Development Center (XO) Arnold Air Force Station, TN 37389		10. PROGRAM ELEMENT, PROJECT, TASK AREA & WORK UNIT NUMBERS Program Element 921E
11. CONTROLLING OFFICE NAME AND ADDRESS National Aeronautics and Space Administration (NASA/JSC), Houston, TX 77058		12. REPORT DATE December 1975 13. NUMBER OF PAGES 50
14. MONITORING AGENCY NAME & ADDRESS *(if different from Controlling Office)*		15. SECURITY CLASS. *(of this report)* UNCLASSIFIED 15a. DECLASSIFICATION/DOWNGRADING SCHEDULE N/A

16. DISTRIBUTION STATEMENT *(of this Report)*

Approved for public release; distribution unlimited.

17. DISTRIBUTION STATEMENT *(of the abstract entered in Block 20, if different from Report)*

18. SUPPLEMENTARY NOTES

Available in DDC.

19. KEY WORDS *(Continue on reverse side if necessary and identify by block number)*

space shuttles	boundary-layer transition
laminar boundary layer	nose bluntness effects
nonequilibrium flow	aerodynamic heating
equilibrium flow	hypersonic flow

20. ABSTRACT *(Continue on reverse side if necessary and identify by block number)*

Inviscid and viscous (laminar boundary layer) flow-field calculations under perfect gas hypersonic wind tunnel and equilibrium real gas flight conditions are presented for the windward centerline of the Rockwell International 139 Space Shuttle Orbiter at 30 deg angle of attack. Correlation parameters for laminar boundary-layer edge quantities and surface heat transfer are developed which properly account for entropy-layer-swallowing effects under both

DD FORM 1 JAN 73 1473 EDITION OF 1 NOV 65 IS OBSOLETE

19, Continued

hypersonic reentry flight
viscous hypersonic flow fields

20, Continued

real and perfect gas conditions. A cursory examination of chemical nonequilibrium effects on the inviscid flow field based on oblique shock relaxation is presented. Some implications of the proposed correlation parameters on boundary-layer transition are discussed.

AFSC
Arnold AFS Tenn

PREFACE

The work reported herein was conducted by the Arnold Engineering Development Center (AEDC), Air Force Systems Command (AFSC), at the request of the National Aeronautics and Space Administration (NASA/JSC), for the Rockwell International Space Division. The results presented were obtained by ARO, Inc. (a subsidiary of Sverdrup & Parcel and Associates, Inc.) contract operator of AEDC, AFSC, Arnold Air Force Station, Tennessee, under ARO Project Numbers VC523 and V43Y-09A. The authors of this report were J. C. Adams, Jr., W. R. Martindale, A. W. Mayne, Jr., and E. O. Marchand, ARO, Inc. The analysis was completed on October 20, 1974, and the manuscript (ARO Control No. ARO-VKF-TR-74-104) was submitted for publication on October 25, 1974.

Acknowledgement and appreciation are extended to D. E. Schramm of Rockwell International Space Division for providing the flight trajectory and wall temperature information used in this study.

CONTENTS

ILLUSTRATIONS

TABLES

Page

1.0 INTRODUCTION

As has been pointed out by Masek and Forney (Ref. 1), two significant problems in the application of existing boundary-layer technology to the National Aeronautics and Space Administration (NASA) Space Transportation System Space Shuttle Orbiter are (1) the choice of a boundary-layer transition criterion and (2) the method used to determine boundary-layer edge conditions. The way in which these problems are solved has a large effect on the resulting surface temperature, heating rate, and heat load distributions along the lower (windward) surface of the vehicle under atmospheric reentry conditions (Ref. 2).

The present work addresses the second of the above-noted problems, i.e., determination of boundary-layer edge conditions for the specific case of hypersonic flow over a blunt-nosed body where account must be taken of entropy-layer swallowing by the boundary layer. As is well known, hypersonic wind tunnel data must be appropriately extrapolated to flight conditions by analytical methods if they are to be effectively utilized in vehicle design. In keeping with this, the primary objective of the present study is the development of correlation parameters which enable perfect gas hypersonic wind tunnel data to be properly scaled to equilibrium real gas flight conditions with respect to laminar boundary-layer edge quantities, including effects of entropy-layer swallowing. A secondary objective is the development of similarity parameters for correlation of surface heat transfer, including effects of entropy-layer swallowing. The physical application of the present study concerns the extrapolation to flight of the 30-deg angle-of-attack laminar boundary-layer edge condition and surface heat-transfer data obtained during the recent NASA/Rockwell International OH9 and OH4B tests conducted in the AEDC von Kármán Gas Dynamics Facility (VKF) Hypersonic Wind Tunnel (B) on the 139 Space Shuttle Orbiter configuration. The approach used in the present work may be summarized as follows:

1. A realistic flow-field model amenable to existing AEDC/VKF analysis techniques was selected.
2. The laminar boundary-layer flow (including entropy-layer swallowing) was calculated for a range of perfect gas wind tunnel and equilibrium real gas flight conditions.
3. The results were correlated in terms of aerodynamic parameters that can be effectively used in design studies.

4. Chemical nonequilibrium effects of the inviscid flow field were estimated in order to assess the applicability of the equilibrium real gas flight calculations.

2.0 FLOW-FIELD MODEL

Calculations from the flow-field model developed in Ref. 3 for sharp-edged delta wings at incidence in hypersonic flow indicate that an angle-of-attack range exists where the windward centerline flow field, both inviscid and viscous, is well approximated by a sharp cone at zero incidence having a half-angle equal to the angle of attack. In the case of an 80-deg-sweep delta wing at free-stream Mach number 9.6, this angle-of-attack range extends from approximately 15 to 33 deg, as shown by Fig. 74 in Ref. 3. The windward surface of the Rockwell International 139 Space Shuttle Orbiter (see Fig. 1) at values of x/L from 0.1 to 0.6

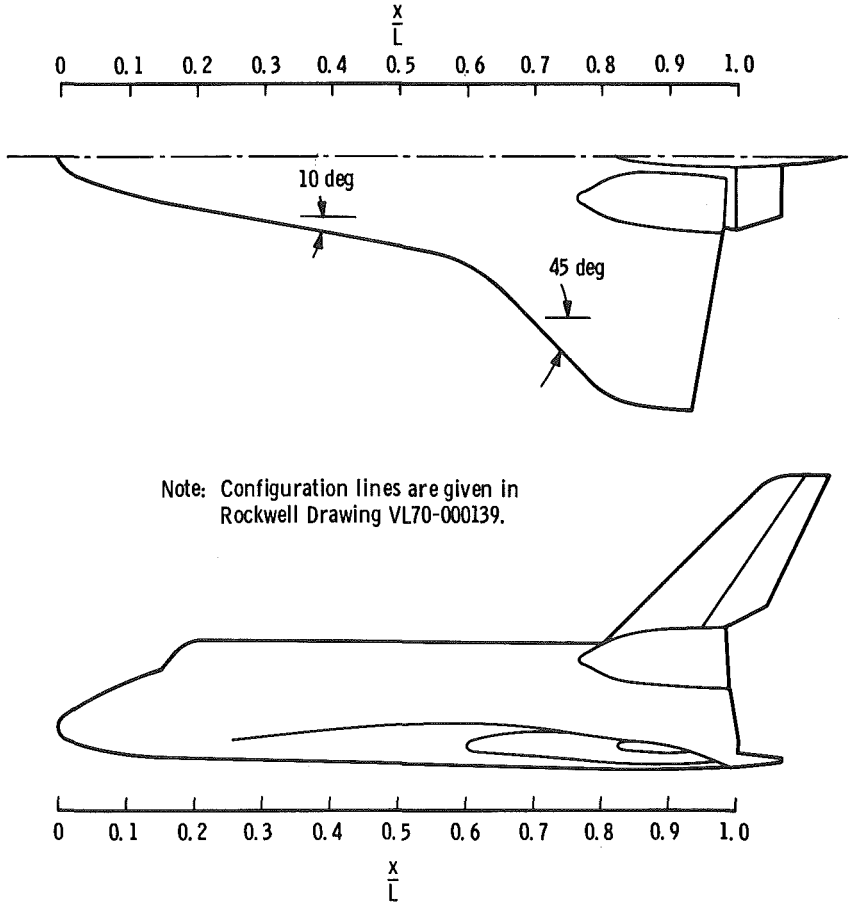

Figure 1. Rockwell International 139 Space Shuttle Orbiter Configuration.

has a relatively flat bottom and a sweep angle of 80 deg. The windward centerline profile has a nearly continuous monotonically decreasing slope from the vehicle nose to an x/L value of 0.25. From this point the slope becomes constant at one degree (with respect to the vehicle reference system) up to an x/L value of 0.8.

Based on the above discussion, a reasonable approximation of the windward centerline flow field for the 139 Space Shuttle Orbiter at 30 deg angle of attack should be an appropriate axisymmetric body at zero incidence. A logical starting point in the search for a matching axisymmetric body is a 31-deg asymptotic half-angle hyperboloid. The continuous geometry of the hyperboloid makes it ideal for numerical flow-field calculations. Use of a trial-and-error method with a model scale drawing showed that a 31-deg hyperboloid with a nose radius to body length value of 0.02635 has an excellent windward centerline profile comparison with the 139 Space Shuttle Orbiter, as shown in Fig. 2. For the full-scale vehicle the values of body length and nose radius are 1290.3 and 34.0 in., respectively; for a 0.0175-scale wind tunnel model, these values become 22.58 and 0.595 in., respectively.

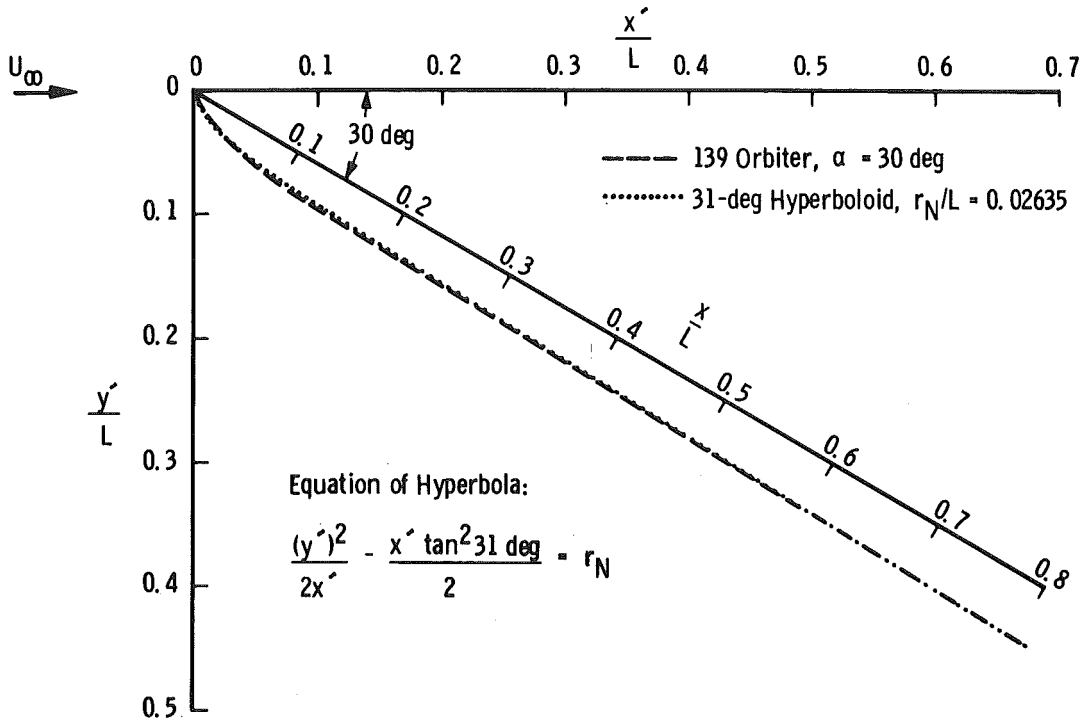

Figure 2. Comparison between 139 Orbiter windward centerline surface profile at 30 deg angle of attack and a 31-deg asymptotic half-angle hyperboloid.

Note that the coordinate system defined in Fig. 2 is aligned with the free-stream velocity vector and that the origin is at the body point where the surface is normal to the free-stream velocity. Also shown in Fig. 2 is the vehicle coordinate x/L. The correspondence of these coordinates and the surface distance coordinate s/r_N is given in Table 1.

Table 1. Coordinate Correspondence

x/L	x'/L	s/r_N
0.003	0	0
0.01	0.0061	0.74
0.02	0.0147	1.27
0.05	0.0407	2.59
0.10	0.0840	4.62
0.15	0.1273	6.59
0.20	0.1706	8.53
0.3	0.2572	12.40
0.4	0.3438	16.25
0.5	0.4304	20.11
0.6	0.5170	23.95
0.7	0.6036	27.79
0.8	0.6902	31.63

Note: α = 30 deg

Now that a matching axisymmetric body at zero incidence has been found, flow-field calculations can be made and compared to hypersonic wind tunnel experimental data to validate the proposed flow-field model. The methods used are described in following sections.

3.0 FLOW-FIELD CALCULATION METHODS

3.1 BOUNDARY LAYER AND INVISCID FLOW

The theory and numerical scheme used in obtaining the present boundary-layer results are based on the work of Patankar and Spalding (Ref. 4). In this approach the classical boundary-layer equations, with

the addition of the transverse curvature terms, are expressed in a normalized von Mises coordinate system and solved by a marching, implicit finite-difference procedure. Although the primary use of the work of Patankar and Spalding has been in the analysis of turbulent boundary layers, the present application is concerned exclusively with laminar boundary layers. Further details concerning the digital computer code and its application are given in a later paragraph.

Since an item of primary interest in the present work is the effect of entropy-layer swallowing on laminar boundary-layer parameters, a discussion of the swallowing process and its analytical treatment is in order. The specification of the conditions along the outer edge of the boundary layer is reasonably straightforward for bodies such as flat plates and sharp cones; however, for the case of a blunt body the problem is more complex. The simplest and, therefore, the most commonly employed method is to first obtain a pressure distribution over the body of interest from an inviscid method-of-characteristics solution or Newtonian theory. Free-stream stagnation conditions behind a normal shock are then determined, and the local flow conditions along the boundary-layer edge are found by isentropically expanding from these stagnation conditions to the known local pressure, thus treating the boundary-layer edge as an isentropic surface. This method is satisfactory for the forward portion of a blunt body; however, as the flow proceeds along the body and the boundary layer grows because of entrainment of mass, the high entropy portion of the flow which crossed the essentially normal portion of the bow shock is swallowed by the boundary layer. The flow along the edge of the boundary layer on the aft portions of the body will then have passed through an oblique part of the bow shock and will be in a different state than had it passed through a normal shock (see Fig. 3).

Assuming the pressure along the outer edge of the boundary layer on a blunt body to have the inviscid surface value*, the determination of the local edge flow conditions may be improved by taking into consideration the inclination of the bow shock where the local flow streamline crossed the shock. The point at which the flow along the edge of the boundary layer crossed the shock can be determined by matching the mass flow in the boundary layer at a given location to the free-stream

*This assumption should be valid as long as the pressure gradient normal to the body surface is small.

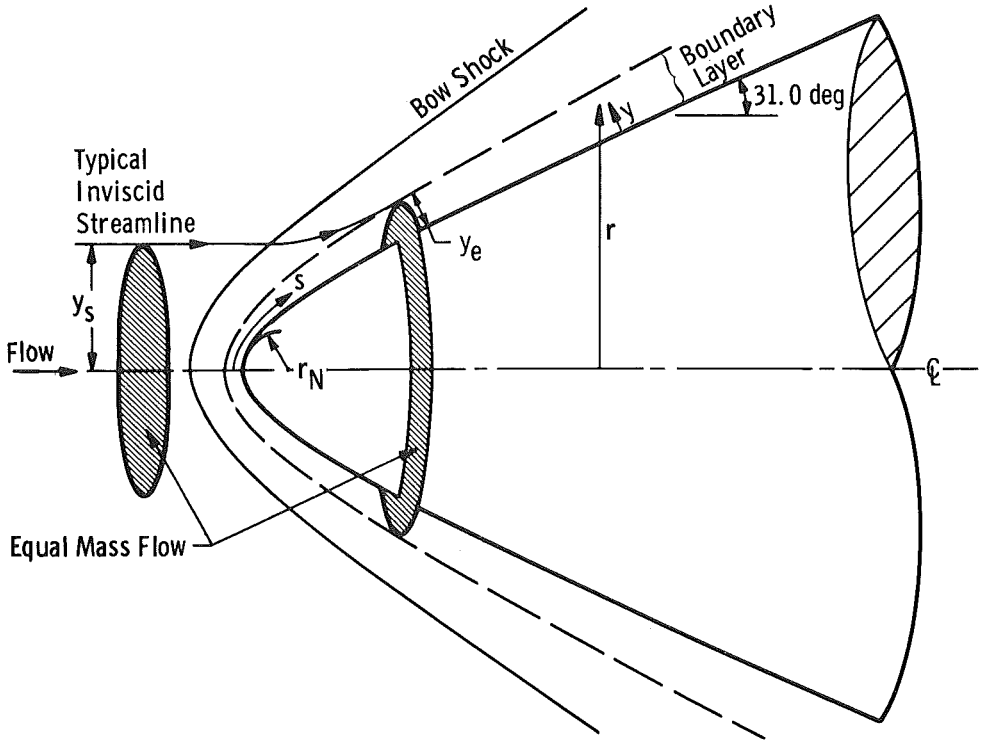

Figure 3. Hyperboloid geometry, showing inviscid streamline swallowing.

mass flow in a cylinder with radius extending out to the location to be determined. Referring again to Fig. 3, this may be expressed as

$$\rho_\infty U_\infty \pi y_s^2 = \int_0^{y_e} 2\pi r \, \rho u \, dy \tag{1}$$

Note that y_e is the thickness of the region over which the boundary-layer equations are being solved. After y_s is found, the shock inclination at that point can be determined and the flow conditions along the boundary layer at the corresponding body location can be computed by crossing the oblique shock at y_s with the free-stream flow and allowing that flow to expand isentropically to the known local boundary-layer edge pressure. Naturally, a swallowing analysis such as described above requires that the shape of the bow shock be known in addition to the body surface pressure. In the present calculations, these data for both real and perfect gas conditions were obtained from a method-of-characteristics solution using the digital computer code developed by Inouye, Rakich, and Lomax (Ref. 5). For the perfect gas cases, the finite-difference method of Aungier (Ref. 6) was used to determine the blunt nose subsonic region solutions for input to the downstream perfect

gas method-of-characteristics analysis. For the real gas (equilibrium air) cases, the inverse method of Lomax and Inouye (Ref. 7) was used to determine the blunt nose subsonic region solutions for input to the downstream real gas method-of-characteristics analysis.

When entropy swallowing is being considered, the definition of the outer edge of the boundary layer must be reconsidered. This is necessary because the velocity and temperature gradients are not zero at the outer edge of the boundary layer but have values associated with the inviscid flow field. This is the result of the combination of the entropy-layer swallowing and the use of the nonsimilar boundary-layer equations. To treat this situation, one may define the boundary-layer thickness in terms of the total enthalpy, since the gradient of this quantity does go to zero at the boundary-layer edge. This approach, proposed by Levine (Ref. 8), was used herein. In particular, the region treated by the boundary-layer equations was adjusted so that y_e was a minimum of 1.1 times the value of y where

$$\frac{H - h_w}{H_\infty - h_w} = 0.999 \tag{2}$$

Consideration of the total enthalpy profile behavior also allows a boundary-layer thickness to be defined in terms of the deviation of H/H_∞ from unity. A total enthalpy boundary-layer thickness, δ_H, has been defined as the distance from the body surface to the point where H/H_∞ differs from unity by 0.005, when approached from the outer part of the flow. For hot-wall cases with overshoot in H/H_∞ (i.e., values greater than one), this means that δ_H is at $H/H_\infty = 1.005$ where $dH/dy \leqslant 0$. For cases with no overshoot, it merely means that δ_H is at $H/H_\infty = 0.995$.

To solve parabolic partial differential equations such as the boundary-layer equations treated herein, it is necessary to specify both the boundary conditions on the dependent variables and the initial values of the dependent variables in the cross-stream direction. Experience has shown that any choice of initial profiles which is not entirely unreasonable can be used with a negligible effect on the downstream results if the computations are begun near the leading edge of a sharp body or the stagnation point of a blunt body. This experience has been used to obtain laminar boundary-layer solutions in the vicinity of the stagnation point of a blunt body by beginning the solution near the stagnation point with assumed profiles and using a number of very small steps in the streamwise direction. With the outer-edge boundary condition determined by the streamline-swallowing

technique given above, the numerical computation proceeds downstream using the marching, implicit finite-difference method of solution discussed previously. Note that this approach properly considers the nonsimilar growth of the boundary layer along the body. In the present analysis, no-slip boundary conditions are applied at the body surface with respect to velocity and temperature.

The computer program used in the present work is written in FORTRAN IV for use on an IBM 370/155 digital computer and is essentially a highly modified version of the code originally devised by Patankar and Spalding (Ref. 4). This program, formulated by Mayne and Dyer (Ref. 9), embodies a number of significant modifications and extensions to the basic technique of Patankar and Spalding. These include elimination of the Couette flow analysis at the body surface and the so-called slip-value scheme in favor of applying the basic finite-difference scheme across the entire boundary layer. The introduction of a variable cross-stream step size which is smaller near the wall than at the outer edge of the boundary layer yields accurate solutions while still permitting the computations to proceed efficiently. Because of the implicit nature of the finite-difference scheme, no numerical stability problems are to be expected from this approach; experience has indicated this to be true.

Calculations for the real gas flight conditions in the present study treat the flow as dissociating air in thermodynamic equilibrium using the thermodynamic and transport property correlation formulas of Cohen (Ref. 10). Under hypersonic wind tunnel conditions, the flow is taken to be thermally and calorically perfect air with a constant Prandtl number of 0.7 in conjunction with Sutherland's viscosity law.

A more complete discussion of entropy-layer swallowing by laminar boundary layers, including comparisons of results from boundary-layer analyses which include and exclude entropy swallowing effects relative to a fully viscous shock layer method, is given by Mayne and Adams in Ref. 11.

3.2 CHEMICAL NONEQUILIBRIUM STREAMTUBE

The theory and numerical scheme used in obtaining the present inviscid chemical nonequilibrium results are based on the work of Adams (Ref. 12) for oblique shock relaxation in air. For a given shock angle, chemically frozen real gas Rankine-Hugoniot oblique shock relations are used to determine the gas state immediately behind the shock. A

chemical nonequilibrium streamtube program based on the implicit integration technique of Lomax and Bailey (Ref. 13) is used to integrate the governing streamtube equations along a constant pressure streamline allowing chemical kinetics to start immediately behind the shock and continue downstream. A schematic of the oblique shock relaxation process is given in Fig. 4.

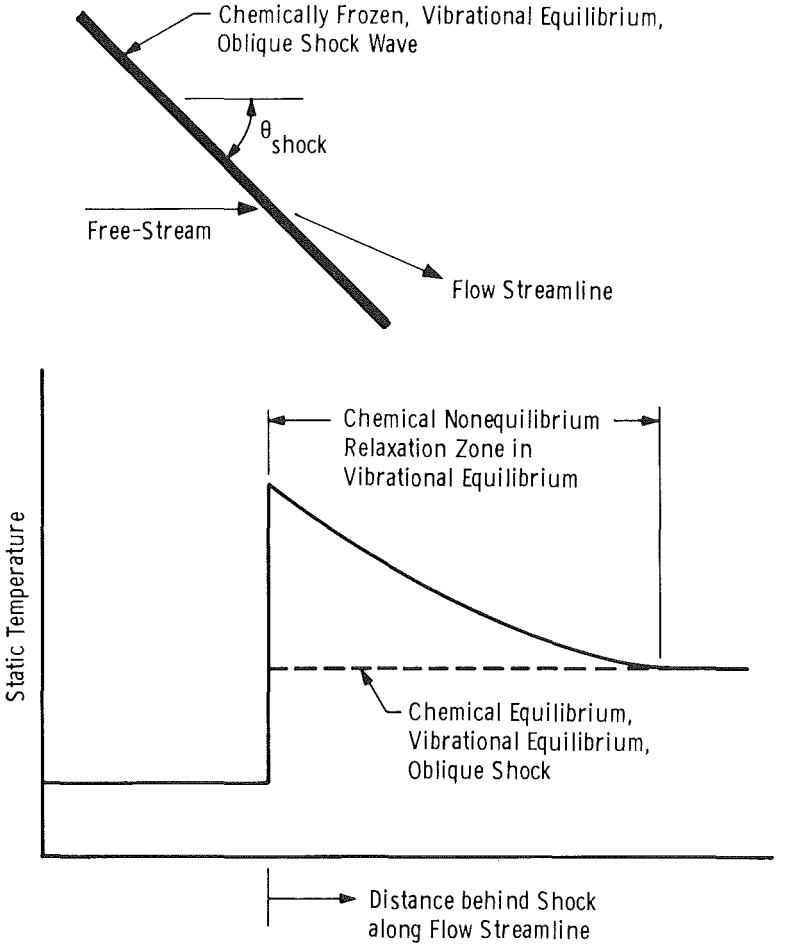

Figure 4. Chemical Nonequilibrium Oblique Shock Relaxation.

The basic gas model is a multicomponent mixture of chemically reacting perfect gases made up of seven species (O, O_2, N, N_2, NO, NO^+, and e^-). The gas is taken to be in vibrational equilibrium but in chemical nonequilibrium, as it is controlled by the chemical kinetic model of dissociating-ionizing air used by Cresswell, et al. (Ref. 14). The seven chemical reactions are given in Table 2; the corresponding forward and backward reaction rates are listed in Table 3, while Table 4 gives the third-body efficiencies for reactions one, two, and

Table 2. Chemical Reactions

1.	$O_2 + M_1$	⇌	$2O + M_1$
2.	$N_2 + M_2$	⇌	$2N + M_2$
3.	$NO + M_3$	⇌	$N + O + M_3$
4.	$NO + O$	⇌	$O_2 + N$
5.	$N_2 + O$	⇌	$NO + N$
6.	$N_2 + O_2$	⇌	$2NO$
7.	$N + O$	⇌	$NO^+ + e^-$

Note: M_i represents any nonreacting collision partner that may be present; data concerning these so-called third bodies are given in Table 4.

Table 3. Reaction Rates

Reaction	Forward Rate			Reverse Rate		
	a	b	E	a	b	E
1	2.5×10^{16}	-0.5	117,945	8.9×10^{14}	-0.44	0
2	2.0×10^{21}	-1.5	225,014	1.91×10^{20}	-1.57	0
3	5.5×10^{20}	-1.5	150,002	1.67×10^{20}	-1.52	0
4	3.2×10^{9}	1.0	39,100	2.67×10^{10}	0.92	7,042.5
5	6.8×10^{13}	0	75,011.5	2.13×10^{13}	-0.04	0
6	6.69×10^{24}	-2.54	128,454	2.4×10^{23}	-2.5	85,500
7	6.4×10^{9}	0.5	64,356.5	7×10^{18}	-0.9	0

Notes: (1) $k = aT^b \exp(-E/\bar{R}T)$

(2) T in °K, $\bar{R}$ = 1.986 cal/gm-mole °K

(3) Units are gm-moles, sec, cm^3, cal, °K

Reference: Cresswell, et al. (Ref. 14)

Table 4. Third-Body Efficiencies*

i	O_2	N_2	N	O	NO
1	5	2	2	25	2
2	2	5	3	5	2
3	2	2	5	5	2

*Multiplicative factors for reaction rates involving nonreacting collision partners, M_i

three in Table 2. Thermodynamic properties (enthalpies and specific heats) for the individual species are taken from Blottner (Ref. 15), whereas the mixture viscosity is obtained from Wilke's formula using individual species properties from Ref. 15.

4.0 FREE-STREAM CONDITIONS

4.1 WIND TUNNEL

Table 5 gives a set of three free-stream conditions in Tunnel B for which data were taken during recent tests of the 139 Orbiter (Ref. 16). The first condition corresponds to the OH9 test where the

Table 5. Tunnel B Conditions

Case	M_∞	Re_∞/ft	Re_{∞, r_N}	$T_{o,\infty}$,°R	Test
1T	7.92	681,614	33,794	1332	OH9
2T	8.00	3,706,270	183,757	1351	OH4B
3T	7.92	541,605	26,853	1263	OH4B

Note: Re_{∞, r_N} is based on a nose radius of 0.04958 ft.

boundary-layer edge conditions were measured via flow-field probe surveys. Model wall temperatures were also measured at this test condition; these values are tabulated in Table 6. The other two free-stream conditions in Table 5 correspond to the maximum and minimum Reynolds number conditions of the OH4B heat-transfer test. It should be noted that these are the maximum and minimum Reynolds numbers available in Tunnel B. Model wall temperatures for these conditions are tabulated in Table 6.

Note the case designation 1T, 2T, and 3T in Tables 5 and 6. This designation will be used in the remainder of this report to identify the wind tunnel conditions.

4.2 FLIGHT

Table 7 gives a set of ten altitude-velocity flight conditions as specified by Rockwell International personnel based upon the Rockwell

Table 6. Model Wall Temperature Ratio Distributions under Tunnel B Conditions

Case / x/L	1T	2T	3T
0.003	0.856	0.415	0.428
0.01	0.766	↓	↓
0.02	0.713		
0.05	0.647		
0.1	0.595		
0.2	0.544		
0.4	0.492		
0.6	0.465		
0.8	0.454		

Note: Above values are $T_w/T_{o,\infty}$ with $T_{o,\infty}$ from Table 5.

Table 7. Rockwell International SSV Trajectory No. 14040

Case	Time, sec	Altitude, ft	Velocity, ft/sec	M_∞	Re_∞/ft	Re_{∞, r_N}
1	400	269,915	26,006	29.41	2,610	7,395
2	496	252,149	25,576	28.01	6,064	17,181
3	608	243,742	24,727	26.38	8,193	23,213
4	704	239,322	23,864	25.14	9,390	26,605
5	800	233,529	22,897	23.73	11,214	31,773
6	896	225,698	21,767	22.09	14,177	40,168
7	1008	212,699	20,119	19.74	20,525	58,154
8	1104	195,803	18,148	17.22	32,755	92,806
9	1200	186,076	15,665	14.70	39,921	113,109
10	1296	178,440	13,310	12.39	44,194	125,216

Notes: (1) Re_{∞, r_N} is based on a nose radius of 2.83333 ft.

(2) For this trajectory 29.5 deg $\leq \alpha \leq$ 31.6 deg; all calculations assume α = 30 deg.

International SSV Trajectory No. 14040. Graphical presentation of this trajectory is given in Fig. 5. The corresponding free-stream properties were taken from the altitude-velocity tables of Ref. 17, which are based on the 1962 U.S. Standard Atmosphere. Note the numerical case designation numbers 1 through 10 in Table 7 and Fig. 5. This designation will be used in the remainder of this report to identify the flight conditions.

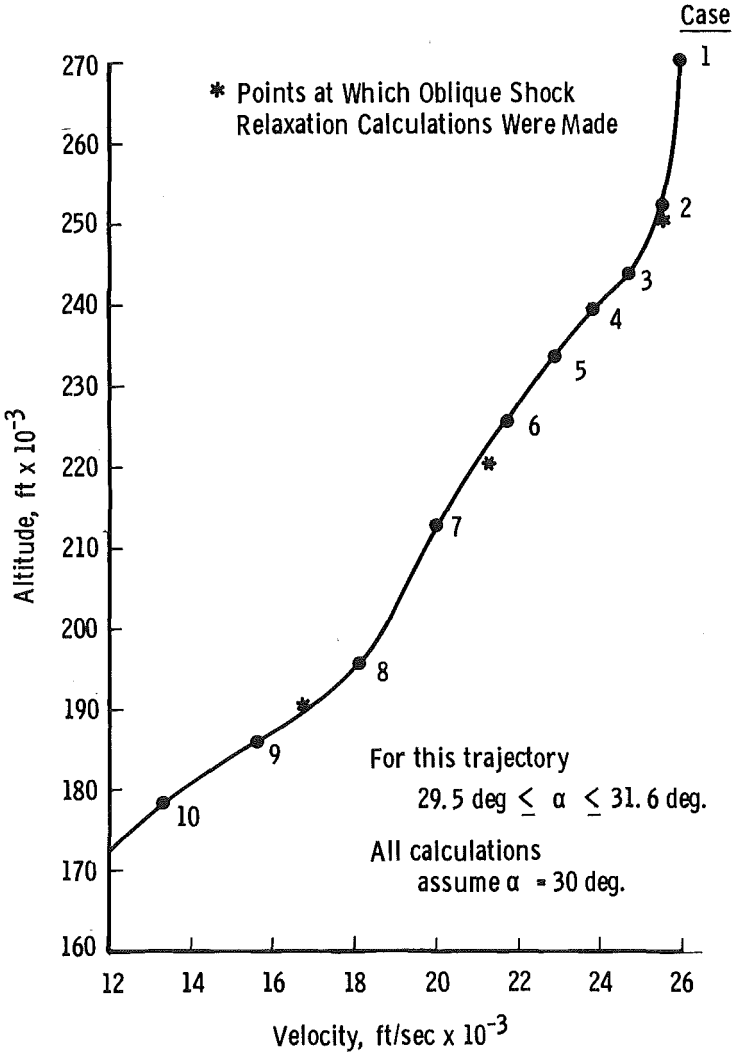

Figure 5. Rockwell International SSV Trajectory No. 14040.

Radiative equilibrium wall temperatures for a laminar boundary layer along the 139 Orbiter windward centerline as specified by Rockwell International personnel based upon the Rockwell International SSV Trajectory No. 14040 are given in Table 8. These wall temperature distributions were input to the boundary-layer calculations to properly take

into account variable wall temperature effects on the entropy-layer swallowing phenomenon under flight conditions.

Table 8. Centerline Radiative Equilibrium Wall Temperature Distributions for Rockwell International SSV Trajectory No. 14040

Case \ x/L	0.005	0.01	0.02	0.05	0.1	0.2	0.4	0.6	0.8
1	2250	2119	1944	1713	1553	1472	1415	1323	1199
2	2533	2392	2199	1944	1782	1726	1661	1553	1412
3	2594	2451	2254	1995	1830	1772	1706	1594	1451
4	2587	2445	2250	1992	1827	1759	1694	1583	1441
5	2585	2444	2250	1993	1828	1751	1688	1577	1435
6	2589	2449	2256	1998	1833	1745	1682	1572	1430
7	2596	2457	2264	2006	1841	1735	1673	1563	1422
8	2590	2454	2263	2007	1843	1718	1657	1547	1408
9	2383	2259	2083	1847	1694	1541	1486	1392	1265
10	2116	2006	1848	1636	1477	1334	1286	1203	1091

Note: Wall temperature values are in °F.

5.0 FLOW-FIELD MODEL VERIFICATION UNDER HYPERSONIC WIND TUNNEL CONDITIONS

In order to verify the applicability of the axisymmetric flow-field model postulated in Section 2.0, comparisons have been made between the present analysis techniques and experimental measurements taken on the 139 Orbiter under the Tunnel B conditions of Tables 5 and 6 as discussed in Section 4.1. Figure 6 presents the measured and calculated inviscid flow-field properties. The surface pressure distribution shown in Fig. 6 reveals relatively good agreement between measured and calculated values. The same is true of the shock shape comparison shown in Fig. 6. Note that the differences between measured and calculated shock shape coordinates are consistent with the differences in body shape coordinates shown previously relative to Fig. 2.

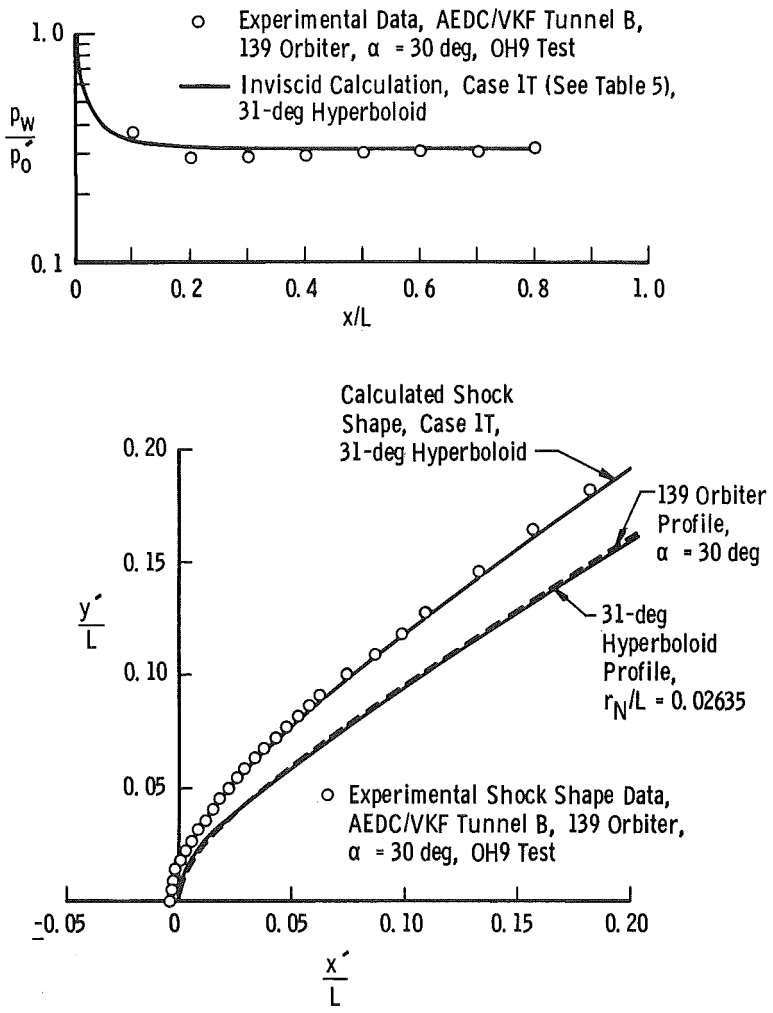

Figure 6. Comparison between hyperboloid surface pressure and shock shape calculations and AEDC/VKF Tunnel B data.

A comparison between measured and calculated (based on the present entropy-layer-swallowing laminar boundary-layer analysis) local boundary-layer edge parameters is given in Fig. 7. The boundary-layer edge is defined as in the discussion in Section 3.1; i.e., all edge conditions (both experimental and calculated) are based on a total enthalpy definition of the boundary-layer thickness, δ_H. Each of the parameters shown in Fig. 7, namely boundary-layer thickness, edge Mach number, and edge Reynolds number, reveals good agreement between experiment and calculations. It is important to observe the entropy-layer-swallowing phenomenon as typified by the edge Mach number and edge Reynolds number distributions relative to the corresponding

limiting values for inviscid conical flow and inviscid normal shock-isentropic expansion. Entropy-layer swallowing is of importance over the entire body for this particular configuration and laminar flow condition.

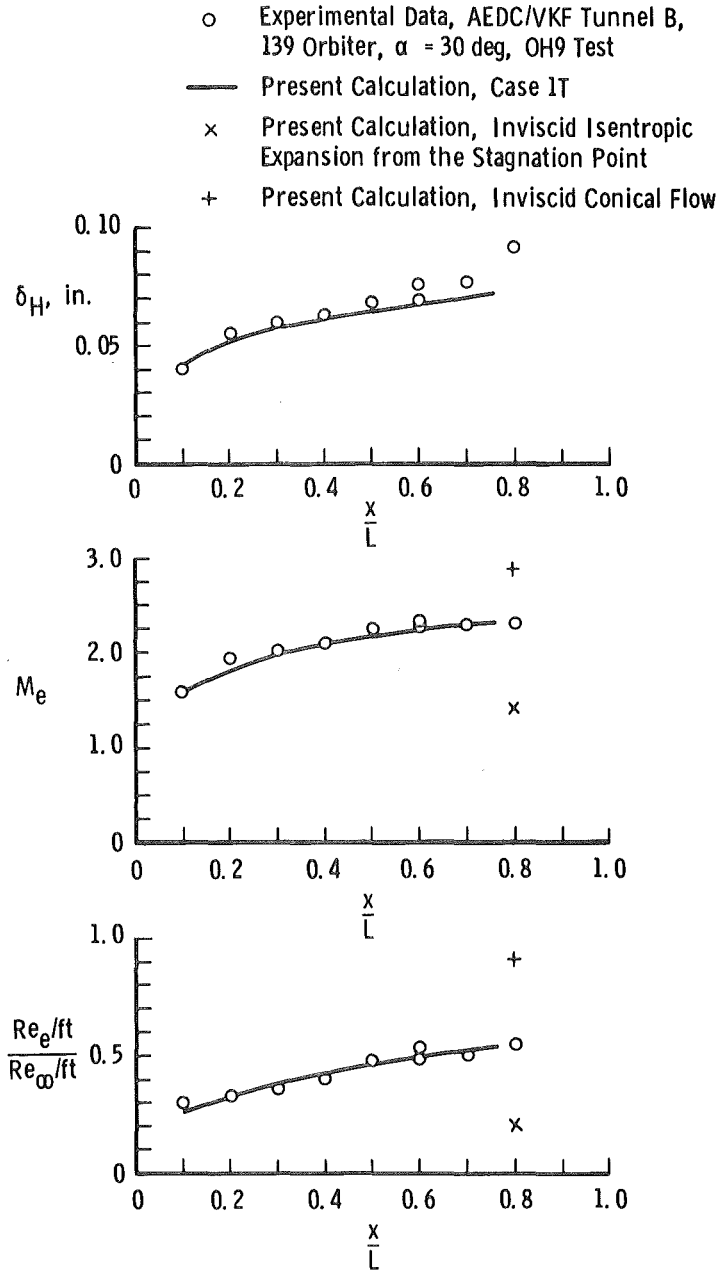

Figure 7. Comparison between hyperboloid boundary-layer edge parameter calculations and AEDC/VKF Tunnel B data.

Calculated and measured boundary-layer profiles are compared in Fig. 8 for the body location x/L = 0.5. Indicated on each figure is the calculated boundary-layer thickness, δ_H, based on the total enthalpy definition. As can be seen from Fig. 8a, pitot pressure measurements alone cannot be used to experimentally define the viscous-inviscid interface (i.e., the boundary-layer thickness) under hypersonic flow conditions where entropy-layer swallowing is important. Total temperature measurements, such as are shown in Fig. 8b, are required for such flows. It should be noted that the experimental measurements shown in Figs. 8a and b have been corrected for pressure lag error and radiation losses, respectively, as described in Ref. 16.

Local Mach number, tangential velocity, and static temperature profiles are presented in Figs. 8c, d, and e, respectively. None of these profiles reveals any indication of boundary-layer thickness under entropy-layer-swallowing conditions. The experimental measurements shown in these figures represent calculated values based

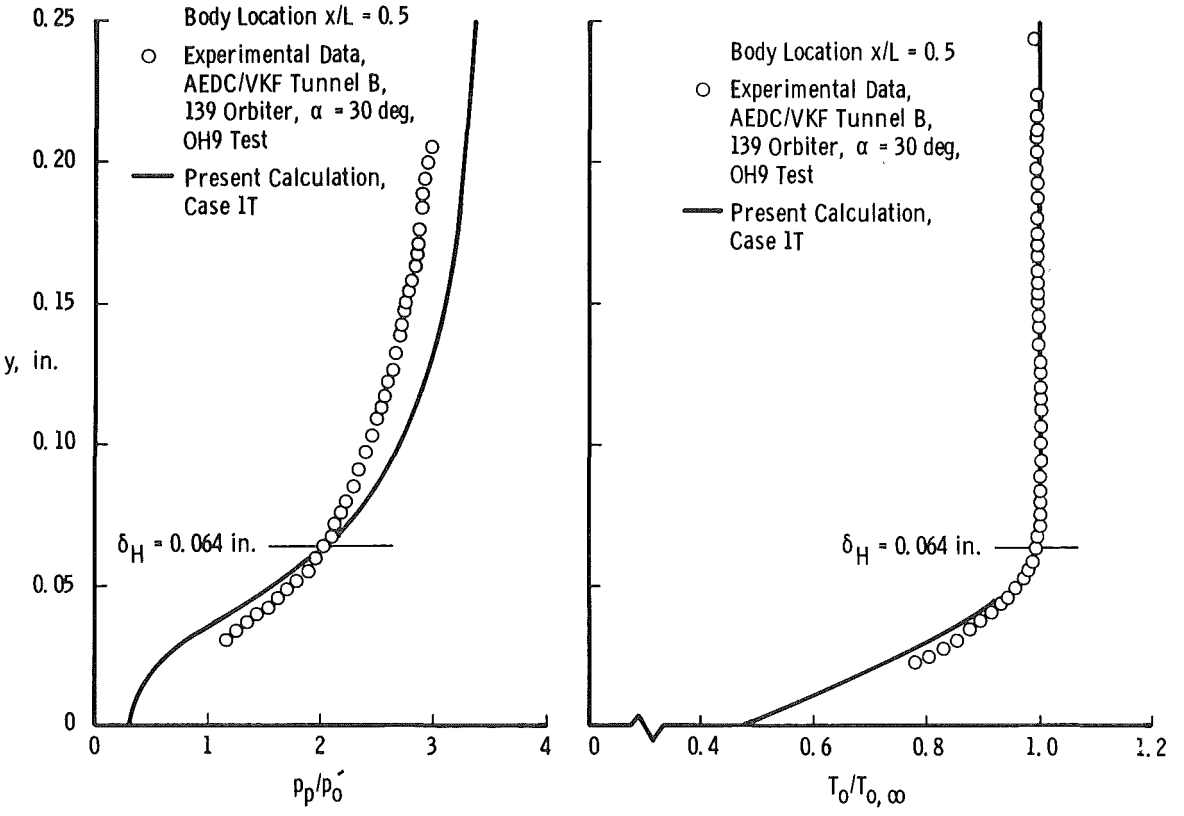

a. Pitot Pressure

b. Total Temperature

Figure 8. Comparison between hyperboloid boundary-layer profile calculations and AEDC/VKF Tunnel B data.

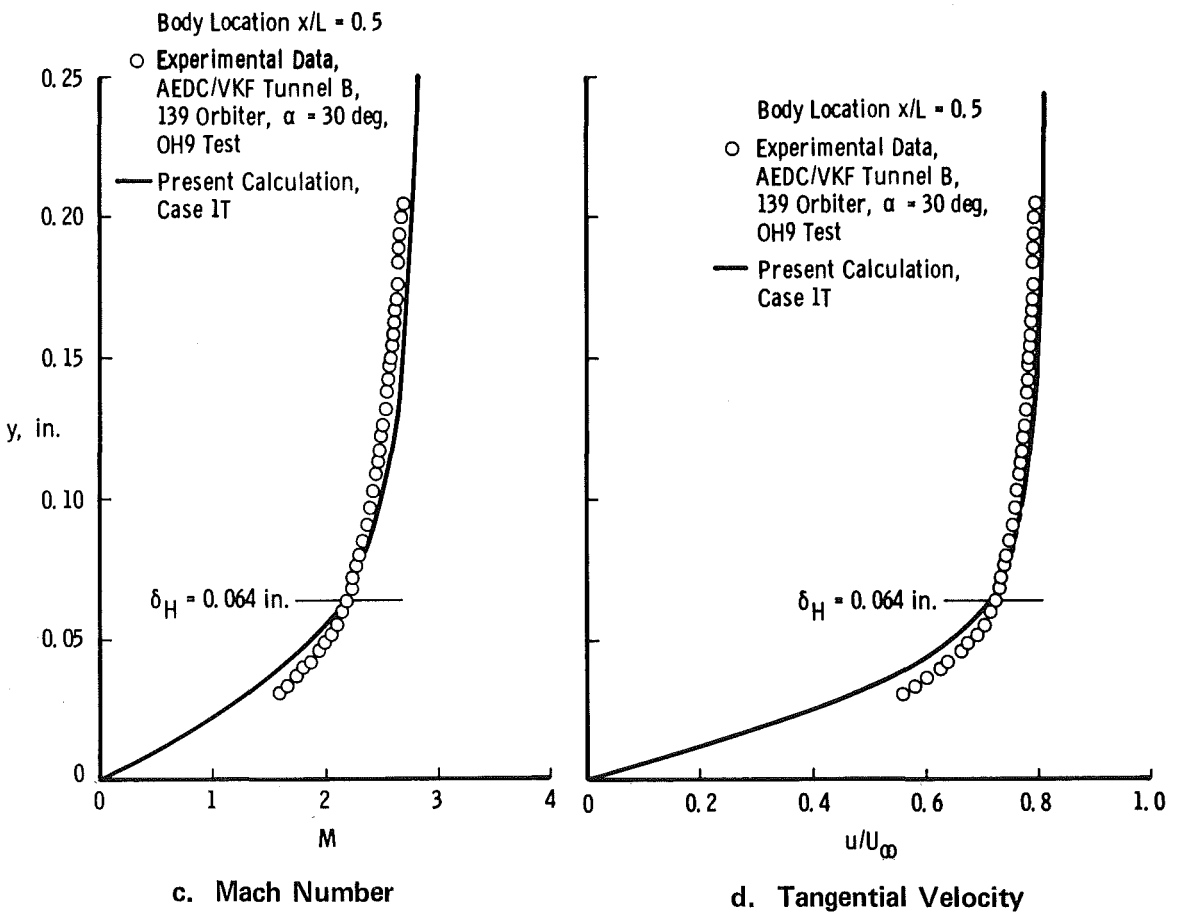

c. Mach Number

d. Tangential Velocity

Figure 8. Continued.

upon the corrected pitot pressure and total temperature measurements of Figs. 8a and b in conjunction with the assumption of constant static pressure normal to the surface.

In general, agreement between calculated and measured profile quantities in Figs. 8a through e is reasonably good. This agreement further illustrates the validity and applicability of the axisymmetric flow-field model under the present hypersonic wind tunnel conditions. This agreement is a direct function of the good shock shape simulation by the hyperboloid geometry shown previously in Fig. 6.

The measured (via the thin-skin thermocouple technique) and calculated surface heat-transfer distributions as reflected through $\bar{h}/\bar{h}_{ref}$ are given in Fig. 9. The comparison is quite good except in the region of $0.15 < x/L < 0.30$ where the measured heat-transfer rates are slightly

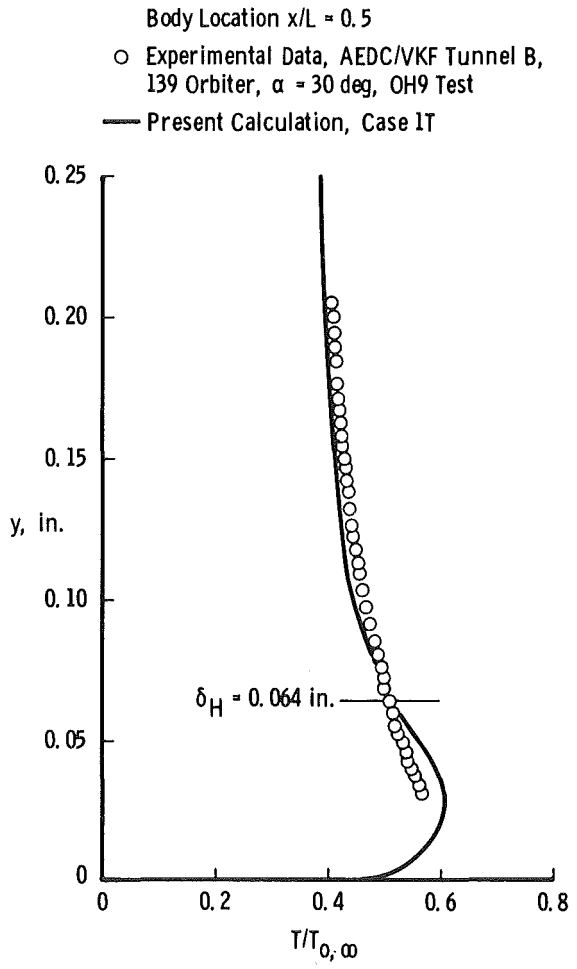

e. Static Temperature
Figure 8. Concluded.

lower than the calculated values. This is consistent with the surface pressure distribution shown previously in Fig. 6.

Note that in the lower portion of Fig. 9 the boundary-layer edge Mach number and edge Reynolds number at the onset of boundary-layer transition are indicated based upon the present entropy-layer-swallowing laminar boundary-layer calculations. In the absence of experimental flow-field data at a particular test condition, an entropy-layer-swallowing boundary-layer calculation is the only way in which these values can be obtained.

The results shown in Figs. 6, 7, 8, and 9 clearly indicate that application of the axisymmetric flow-field model developed in Section 2.0 and

the entropy-layer-swallowing boundary-layer calculation methods presented in Section 3.1 results in realistic values of measurable flow-field and surface parameters for the 139 Orbiter at 30 deg angle of attack under hypersonic wind tunnel conditions. It is therefore reasonable to assume that, by using equilibrium air properties in the present calculation methods, realistic flow-field calculations can be obtained under real gas flight conditions, if the flow is indeed close to equilibrium.

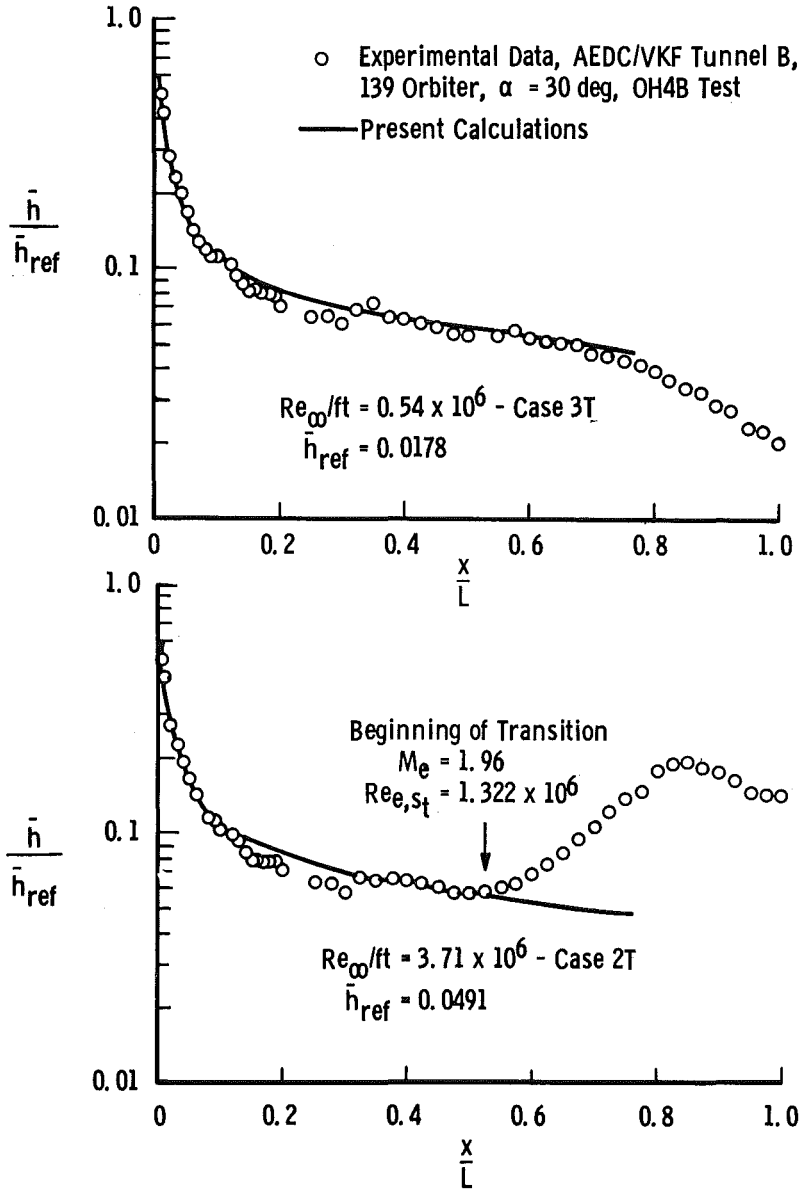

Figure 9. Comparison between hyperboloid surface heat-transfer calculations and AEDC/VKF Tunnel B data.

6.0 CORRELATION OF BOUNDARY-LAYER PARAMETERS INCLUDING EFFECTS OF ENTROPY-LAYER SWALLOWING

As stated in Section 1.0, the most important objective of the present investigation is the development of correlation parameters which enable hypersonic wind tunnel data to be properly scaled to flight with respect to laminar boundary-layer edge quantities under flow conditions where entropy-layer swallowing must be taken into account. Of secondary importance is the development of laminar boundary-layer heat-transfer parameters which properly reflect entropy-layer swallowing effects. In both cases the chosen parameters must be simple to use (in an engineering sense) and accurately account for real gas effects as encountered in flight.

Following Rotta and Zakkay (Ref. 18), whose work is based on earlier work by Ferri (Ref. 19), Zakkay and Krause (Ref. 20), and Rubin (Ref. 21), there is sound theoretical justification for choosing the following form of a similarity parameter (denoted hereafter as S) for the entropy-layer-swallowing process

$$S = \frac{s/r_N}{Re_{\infty,r_N}^{1/3}} \tag{3}$$

where s is surface distance from the stagnation point (see Fig. 3), r_N is the nose radius of the body, and Re_{∞, r_N} is the free-stream Reynolds number based on the nose radius, r_N. The 1/3 power on Re_{∞, r_N} in the denominator of Eq. (3) is due to the theoretical analysis of Ref. 18 as mentioned above. As noted in Ref. 18, the dependence of the laminar boundary-layer outer edge properties on the nose radius vanishes when these properties are expressed in terms of the similarity parameter S under flow conditions where entropy-layer swallowing is important. A similar finding holds with respect to laminar boundary-layer heat transfer, as shown in Ref. 19. It is to be emphasized that Eq. (3) represents a similarity parameter for the entropy-swallowing process on axisymmetric bodies of revolution at zero angle of attack under either real or perfect gas conditions, as can be seen by reference to the theoretical analysis on pp. 508-509 of Ref. 18. The similarity parameter, S, is not applicable in the nose region of the body; neither is it applicable for very low Reynolds number flows. The correspondence of physical surface distance, s, for a given value of S is given in Fig. 10 for both the wind tunnel and flight conditions (Tables 5 and 7, respectively) of current interest. Because of the above statement that

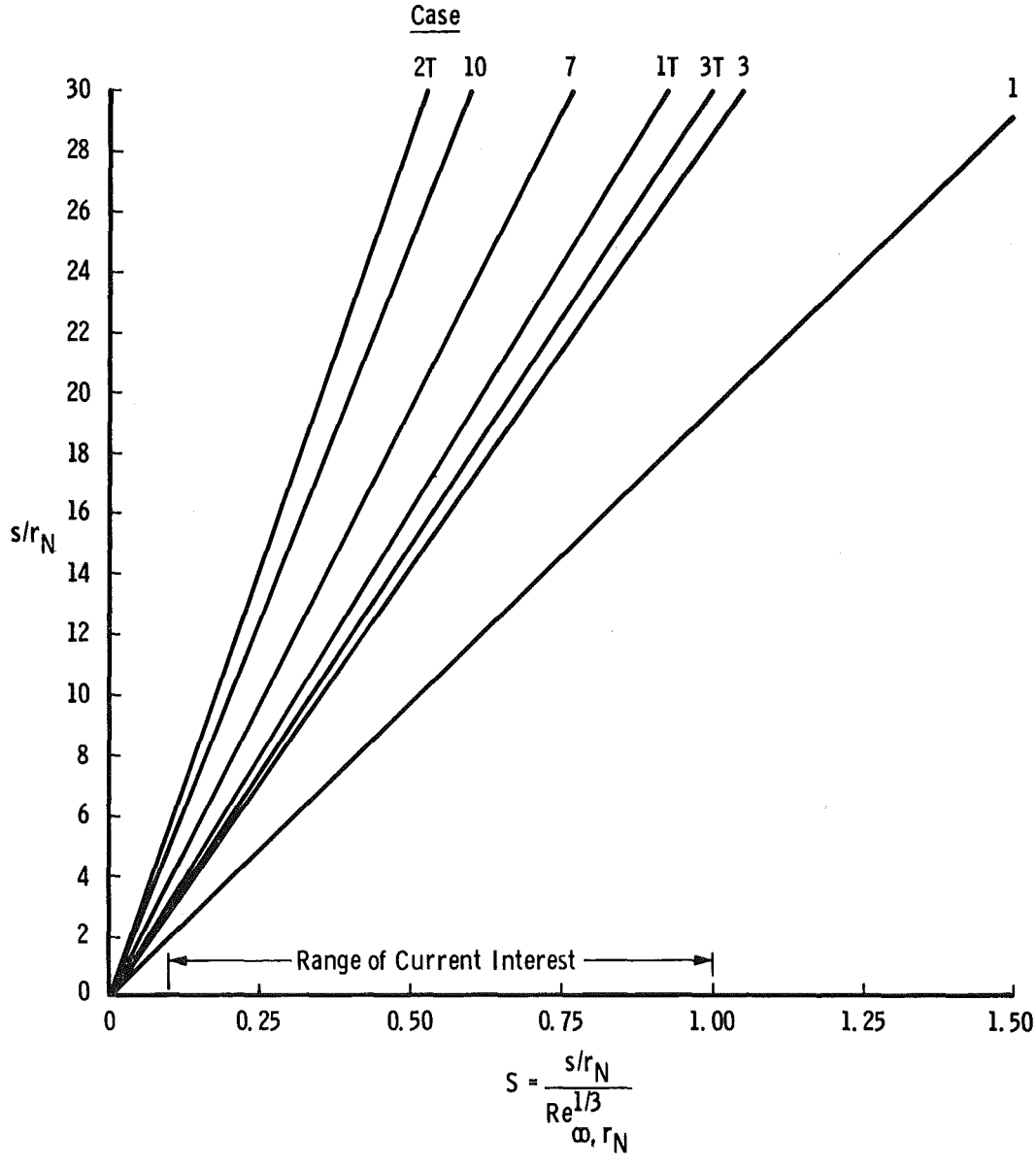

Figure 10. Correspondence of physical surface distance, s, for a given value of the similarity parameter, S.

the similarity parameter, S, is not applicable in the nose region of the body or for very low Reynolds number flows, it is assumed that the range of current interest as indicated in Fig. 10, namely $0.10 \leq S \leq 1.0$, is a reasonable choice for the present flow conditions. All succeeding figures which employ the similarity parameter, S, will be restricted to this range.

Examination of the calculated results for flight cases 1 through 10 and wind tunnel cases 1T through 3T has revealed the following correlation parameters for the outer edge boundary-layer parameters:

Outer Edge Quantity	Correlation Parameter
M_e	$\frac{M_e / M_{e,\,NS}}{M_{conical}}$
Re_e/ft	$\frac{(Re_e/ft)/(Re_{e,\,NS}/ft)}{M_\infty^{0.70}}$

Here, the subscript NS denotes the so-called normal shock outer edge condition which, for a given body location, is obtained by isentropically expanding the body surface inviscid flow from the stagnation point to the local surface pressure. The conical Mach number, $M_{conical}$, is based upon the inviscid sharp cone surface Mach number as tabulated in Table 9 for both real gas flight conditions and perfect gas wind tunnel conditions; note that the sharp cone is a 31-deg half-angle type, which corresponds to the asymptotic half-angle of the hyperboloid. Use of the

Table 9. Conical Mach Number Based on Inviscid Solution for a 31-deg Half-Angle Sharp Cone.

Case	Type Gas	$M_{conical}$
1	Real	5.202
2		5.085
3		4.993
4		4.987
5		5.051
6		5.070
7		4.919
8		4.631
9		4.220
10		3.782
1T-3T	Perfect	2.887

so-called normal shock outer edge conditions in a normalized sense represents an attempt to reduce the real gas effects on the resulting parameter; the free-stream Mach number and the conical Mach number represent a further attempt to account for free-stream Mach number effects. The power of unity on the conical Mach number and 0.70 on the free-stream Mach number are the results of plotting $M_e/M_{e,NS}$ [or $(Re_e/ft)/(Re_{e,NS}/ft)$] versus $M_{conical}$ (or M_∞) at a common value of the similarity parameter, S, for both the flight and wind tunnel cases.

Logarithmic plots which show a data band encompassing flight cases 1 through 10 and wind tunnel cases 1T through 3T are presented in Figs. 11 and 12 for the outer edge Mach number and outer edge Reynolds number correlation parameters, respectively. A mean fit to the data band

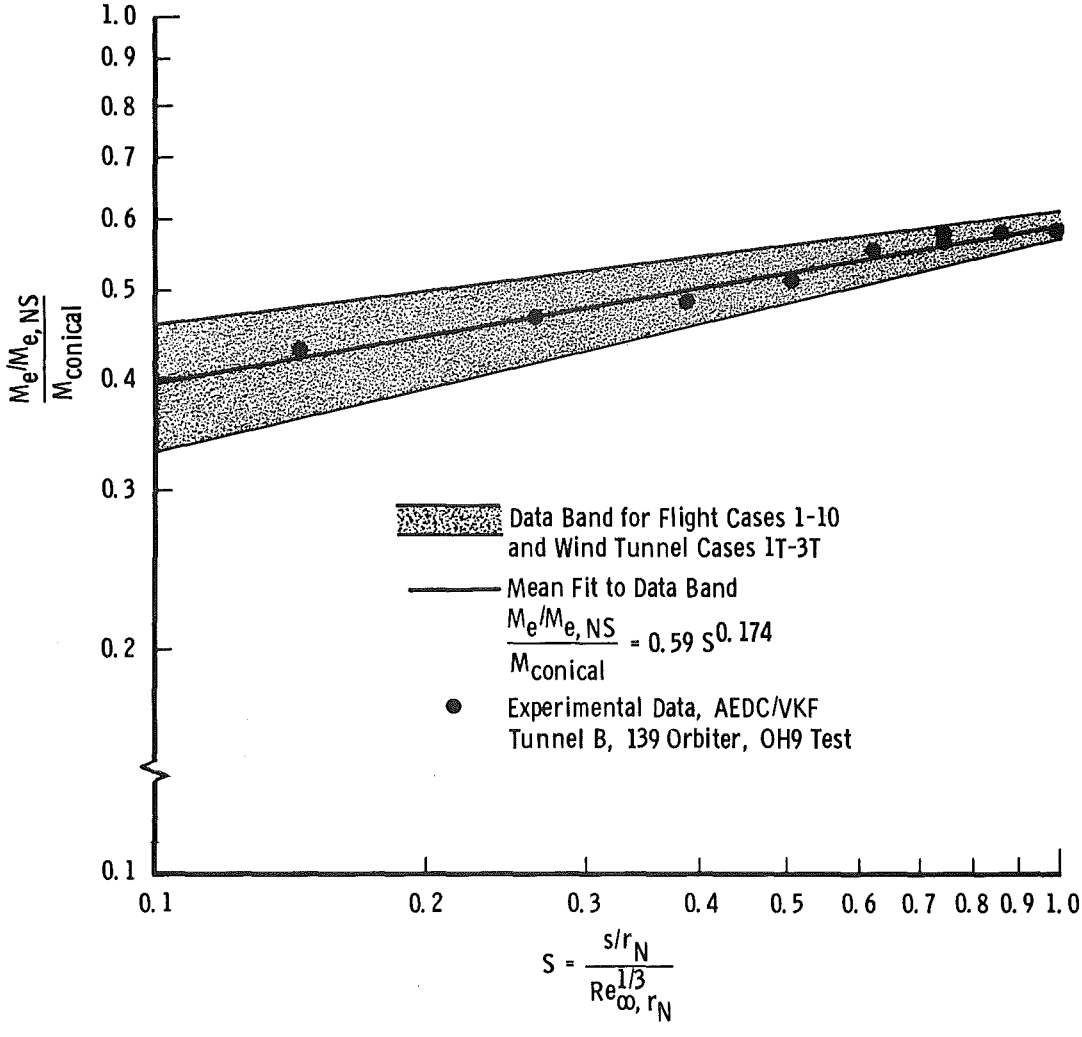

Figure 11. Logarithmic plot of the laminar boundary-layer outer edge Mach number correlation parameter.

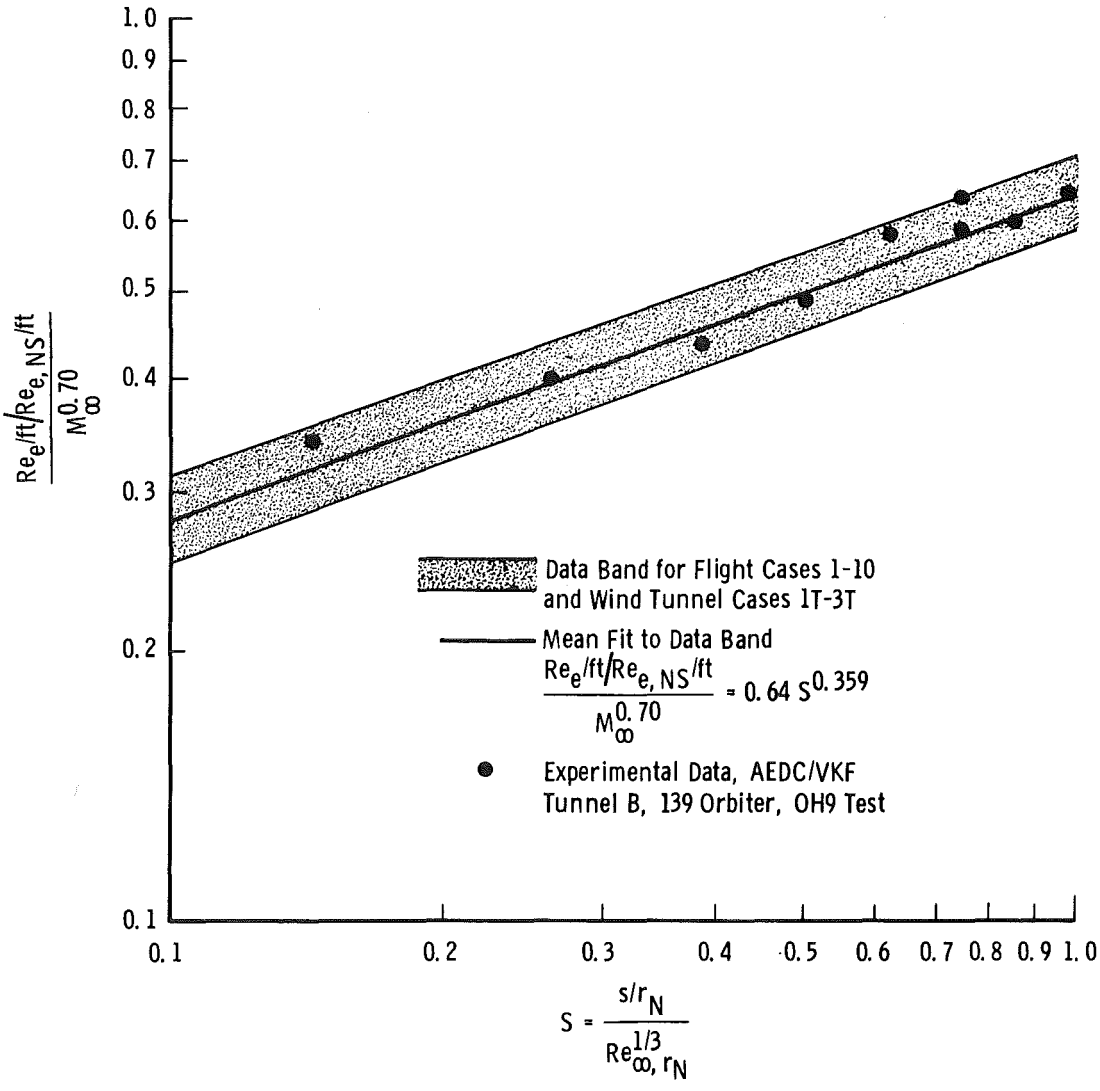

Figure 12. Logarithmic plot of the laminar boundary-layer outer edge unit Reynolds number correlation parameter.

is shown on each figure along with the resulting numerical constants for the mean fit. Also indicated by closed circles on the figures are the experimental data from the Tunnel B flow-field survey along the windward centerline of the 139 Orbiter. It is important to observe from Figs. 11 and 12 that the maximum deviation from the mean fit to the data band is only approximately ±10 percent, which clearly reveals the applicability of the presently proposed correlation parameters under both real gas flight conditions and perfect gas wind tunnel conditions.

Under hypersonic flow conditions where entropy-layer swallowing effects are important, classical laminar boundary-layer parameters such as displacement thickness and momentum thickness become ill-defined due to gradients in the boundary-layer velocity and static density profiles at the outer edge of the boundary layer. A boundary-layer parameter which has physical meaning under these conditions is a boundary-layer thickness based upon the total enthalpy definition of the boundary-layer edge, as discussed previously in Section 3.1. Classical laminar boundary-layer theory for a sharp cone at zero angle of attack in a supersonic or hypersonic flow indicates that the boundary-layer thickness, δ, is given by an expression of the form

$$(\delta/s')\sqrt{Re_{e,s'}} = f(M_\infty, \text{etc.}) \tag{4}$$

where s′ is surface distance from the apex of the cone. In an analogous manner, it is reasonable to postulate that the laminar boundary-layer thickness, δ_H, based on a total enthalpy definition under conditions where entropy-layer swallowing is important can be correlated by an expression of the form

$$(\delta_H/s)\sqrt{Re_{e,s}} = f(M_\infty, \text{etc.}) \tag{5}$$

which can be written as

$$\frac{(\delta_H/r_N)\sqrt{Re_{e,r_N}}}{Re_{\infty,r_N}^{1/6}} = f(M_\infty, \text{etc.}) \sqrt{\frac{s/r_N}{Re_{\infty,r_N}^{1/3}}} = f(M_\infty, \text{etc.})\sqrt{S} \tag{6}$$

where Re_{e,r_N} is based upon the local value of Re_e/ft corresponding to the local value of the similarity parameter, S. A logarithmic plot of the above-proposed correlation parameter for total enthalpy-defined boundary-layer thickness is given in Fig. 13 as a function of all ten real gas flight conditions and the three perfect gas wind tunnel conditions. A weak free-stream Mach number influence on the correlation parameter is shown in Fig. 13, namely

$$\frac{(\delta_H/r_N)\sqrt{Re_{e,r_N}}}{Re_{\infty,r_N}^{1/6}\, M_\infty^{0.058}} \tag{7}$$

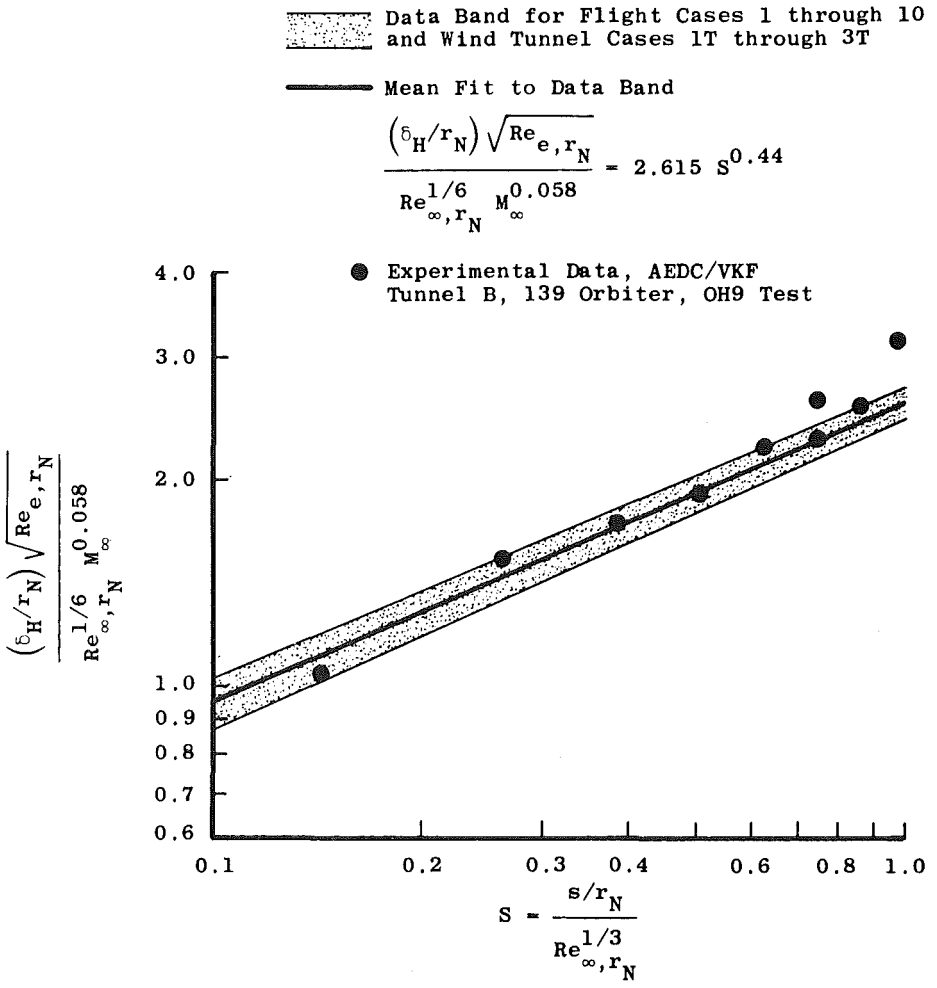

Figure 13. Logarithmic plot of the laminar boundary-layer thickness correlation parameter.

which is based upon examination of the free-stream Mach number effect at a common value of the similarity parameter, S. Examination of Fig. 13 reveals that the above-proposed correlation parameter for total enthalpy-defined boundary-layer thickness yields correlated results within ±10 percent maximum deviation from the mean fit to the data band for both real gas flight conditions and perfect gas wind tunnel conditions. Note also that Fig. 13 contains the experimental data (indicated by closed circles) from the Tunnel B flow-field survey along the windward centerline of the 139 Orbiter.

Let us now turn our attention to development of a surface heat-transfer correlation parameter under flow conditions where entropy-layer swallowing effects are important. Classical laminar boundary-

layer theory for a sharp cone at zero angle of attack in a hypersonic flow under cold wall conditions indicates that the surface heat transfer is given by an expression of the form

$$St_e \sqrt{Re_{e,s'}} = f(M_\infty, \text{etc.}) \tag{8}$$

where s′ is surface distance from the apex of the sharp cone and St_e is a Stanton number based on local edge and wall conditions; i.e.,

$$St_e = \frac{-\dot{q}_w}{\rho_e U_e (H_\infty - h_w)} \tag{9}$$

In an analogous manner, it is reasonable to postulate that the laminar boundary-layer surface heat transfer under conditions where entropy-layer swallowing is important can be correlated by an expression of the form

$$St_e \sqrt{Re_{e,s}} = f(M_\infty, \text{etc.}) \tag{10}$$

which can be written as

$$St_e \sqrt{Re_{e,r_N}}\ Re_{\infty,r_N}^{1/6} = \frac{f(M_\infty, \text{etc.})}{\sqrt{\frac{s/r_N}{Re_{\infty,r_N}^{1/3}}}} = \frac{f(M_\infty, \text{etc.})}{\sqrt{S}} \tag{11}$$

where Re_{e,r_N} is based on the local value of Re_e/ft corresponding to the local value of the similarity parameter, S. In the evaluation of the Stanton number

$$St_e = \frac{-\dot{q}_w}{\rho_e U_e (H_\infty - h_w)} \tag{12}$$

the value of the local edge mass flux, $\rho_e U_e$, must be determined in a manner consistent with the local value of Re_e/ft; in addition, the local value of the wall enthalpy, h_w, corresponding to the local value of the similarity parameter, S, must be used for nonuniform wall enthalpy conditions,

Determination of the local edge mass flux $\rho_e U_e$ in a manner consistent with the local value of Re_e/ft is a subtle point, especially for real gas flow conditions. The following iterative calculation procedure

is suggested to determine a consistent value of $\rho_e U_e$ under real gas conditions:

1. Find $Re_e/ft = \rho_e U_e/\mu_e$ at a given value of $S = (s/r_N)/Re_{\infty, r_N}^{1/3}$ from the correlation curve.

2. Guess a value for U_e (a reasonable first guess is $U_e = U_\infty \cos \alpha$) and calculate h_e from constancy of total enthalpy, namely $h_e = H_\infty - 1/2\ U_e^2$.

3. Note that for a real gas (equilibrium air), the Cohen (Ref. 10) correlation functions give $\rho_e = f_1(p_w, h_e)$ and $\rho_e\mu_e = f_2(p_w, h_e)$ where the local value of the surface pressure p_w is used consistent with the value of S.

4. With U_e, ρ_e, and $\rho_e\mu_e$ determined by the above procedure, compute

$$Re_e/ft = \frac{\rho_e U_e}{\mu_e} = \frac{\rho_e^2 U_e}{\rho_e \mu_e}$$

and compare the resulting value with the value from step (1) above. Iterate on value of U_e using steps (2), (3), and (4) until the procedure converges to consistent values of Re_e/ft from steps (1) and (4).

Under perfect gas wind tunnel conditions, exactly the same calculation procedure is used except that in step (3) the perfect gas equation of state is used to determine ρ_e and Sutherland's viscosity law is used to determine μ_e.

A logarithmic plot of the above proposed correlation parameter for surface heat transfer is given in Fig. 14 as a function of all ten real gas flight conditions and the three perfect gas wind tunnel conditions. It is to be noted that no free-stream Mach number effect could be discerned from examination of the data in the manner discussed previously. As can be seen from Fig. 14, the above proposed correlation parameter for surface heat transfer yields correlated results within ±5 percent maximum deviation from the mean fit to the data band for both real gas flight conditions and perfect gas wind tunnel conditions. The key points in this successful application are the determination of the local mass flux $\rho_e U_e$ per the above discussion and the use of the local wall enthalpy in the Stanton number expression.

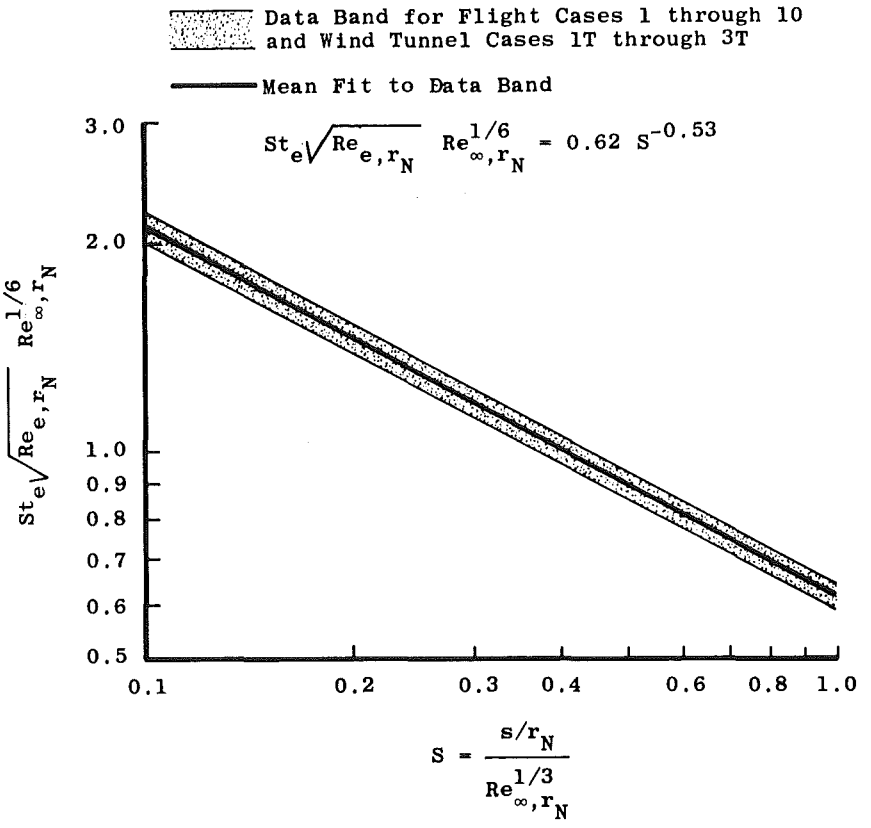

Figure 14. Logarithmic plot of the laminar boundary-layer surface heat-transfer correlation parameter.

A summary of the presently proposed laminar boundary-layer correlation parameters under entropy-swallowing conditions is given in Table 10. As shown above, these parameters are applicable under real gas flight conditions as well as perfect gas wind tunnel conditions. Through use of these parameters, laminar boundary-layer probe survey data and surface heat-transfer data taken in a hypersonic wind tunnel can be properly scaled to flight conditions with respect to boundary-layer outer edge parameters, boundary-layer thickness, and surface heat transfer under flow conditions where entropy-layer swallowing is important.

7.0 ESTIMATE OF CHEMICAL NONEQUILIBRIUM EFFECTS ON OUTER EDGE PARAMETERS

All of the foregoing analysis relative to flight conditions is based upon the assumption of thermochemical equilibrium in both the inviscid

Table 10. Summary of Proposed Correlation Parameters under Entropy-Layer-Swallowing Conditions.

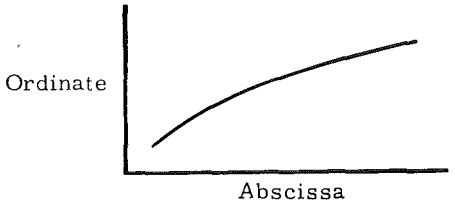

Abscissa	Ordinate
$S = \dfrac{s/r_N}{Re_{\infty, r_N}^{1/3}}$	$\dfrac{M_e/M_{e,NS}}{M_{conical}}$
	$\dfrac{Re_e/ft/Re_{e,NS}/ft}{M_\infty^{0.70}}$
	$\dfrac{(\delta_H/r_N)\sqrt{Re_{e,r_N}}}{Re_{\infty,r_N}^{1/6} M_\infty^{0.058}}$
	$St_e \sqrt{Re_{e,r_N}}\ Re_{\infty,r_N}^{1/6}$

and viscous flow fields. In order to examine the effects of chemical nonequilibrium on boundary-layer outer edge parameters under flight conditions, a series of calculations has been performed for the case of oblique shock relaxation in air using the chemical nonequilibrium streamtube analysis described in Section 3.2 of the present report. Three sets of altitude-velocity conditions have been considered, namely

Altitude, ft	Velocity, ft/sec
250,000	25,600
220,000	21,300
190,000	16,700

which are reasonably close to the Rockwell International SSV Trajectory No. 14040 given in Table 7 and shown in Fig. 5. At each of these altitude-velocity conditions, three shock angles have been considered, namely θ_{shock} = 35, 45, and 55 deg where θ_{shock} is defined as in Fig. 4. This choice of shock angles is designed to simulate inviscid streamline swallowing under chemical nonequilibrium conditions. For example,

θ_{shock} = 35 deg represents a fully swallowed streamline on a body at approximately 31 or 32 deg angle of attack; θ_{shock} = 55 deg represents a typical streamline in the region where swallowing phenomena are important.

Summary plots of the local Mach number and local unit Reynolds number are given in Figs. 15 and 16 for the three altitude-velocity conditions of present interest. Also shown in these figures are equilibrium air results for the same shock angles and flow conditions. It is to be noted that the local Mach number is defined in terms of the so-called frozen speed of sound under chemical nonequilibrium conditions and the equilibrium speed of sound under chemical equilibrium conditions; see Section 5 in Chapter VIII of Vincenti and Kruger (Ref. 22) for an excellent discussion of frozen and equilibrium speeds of sound. As can be seen from Fig. 15, chemical nonequilibrium effects on the local Mach number are almost insignificant, especially for the higher shock angles. A more significant chemical nonequilibrium effect is shown in Fig. 16 with respect to the local unit Reynolds number. For the 35-deg shock angle condition, the equilibrium value of the local unit

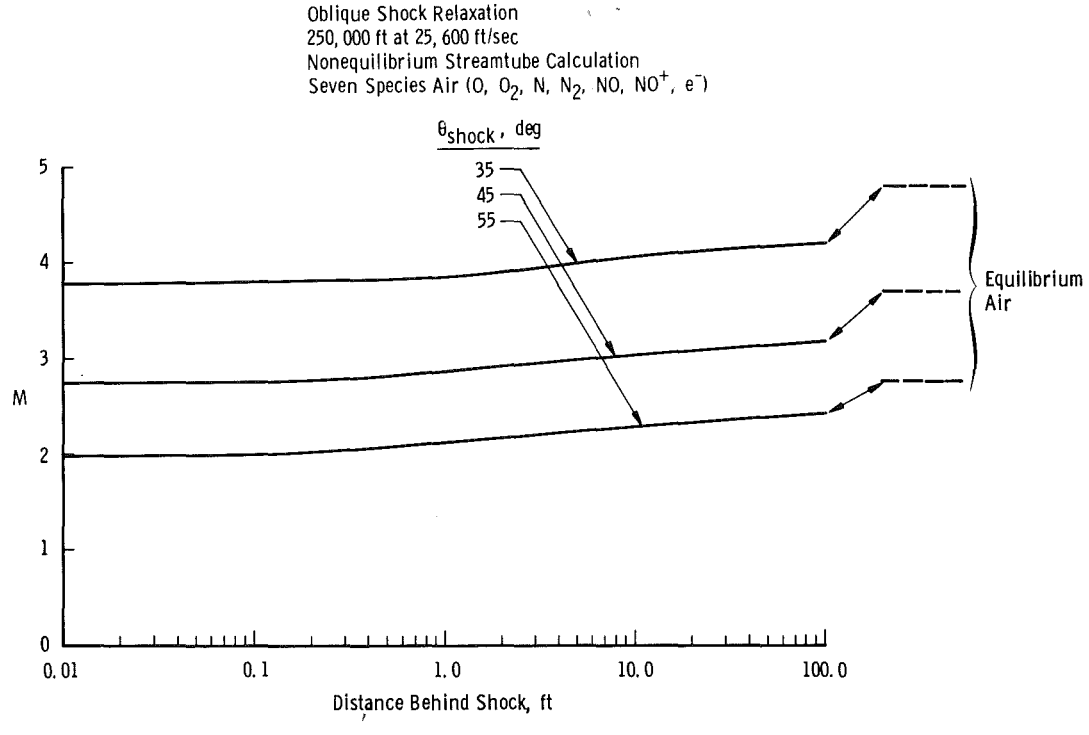

a. 250,000 ft at 25,600 ft/sec

Figure 15. Chemical nonequilibrium oblique shock relaxation effects on the local Mach number.

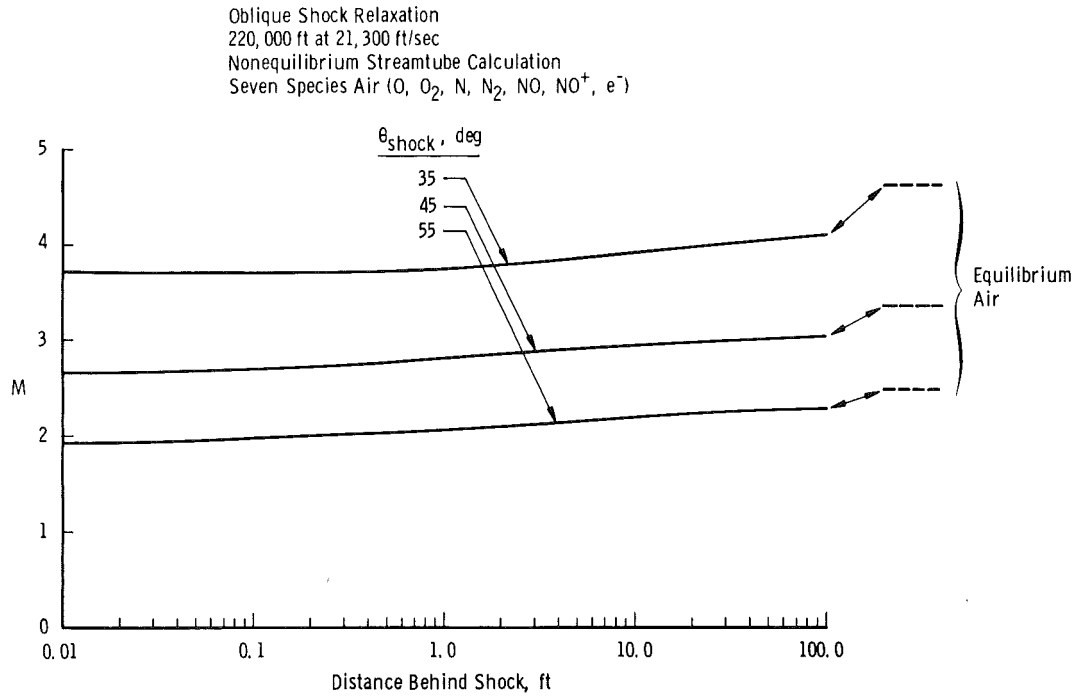

b. 220,000 ft at 21,300 ft/sec

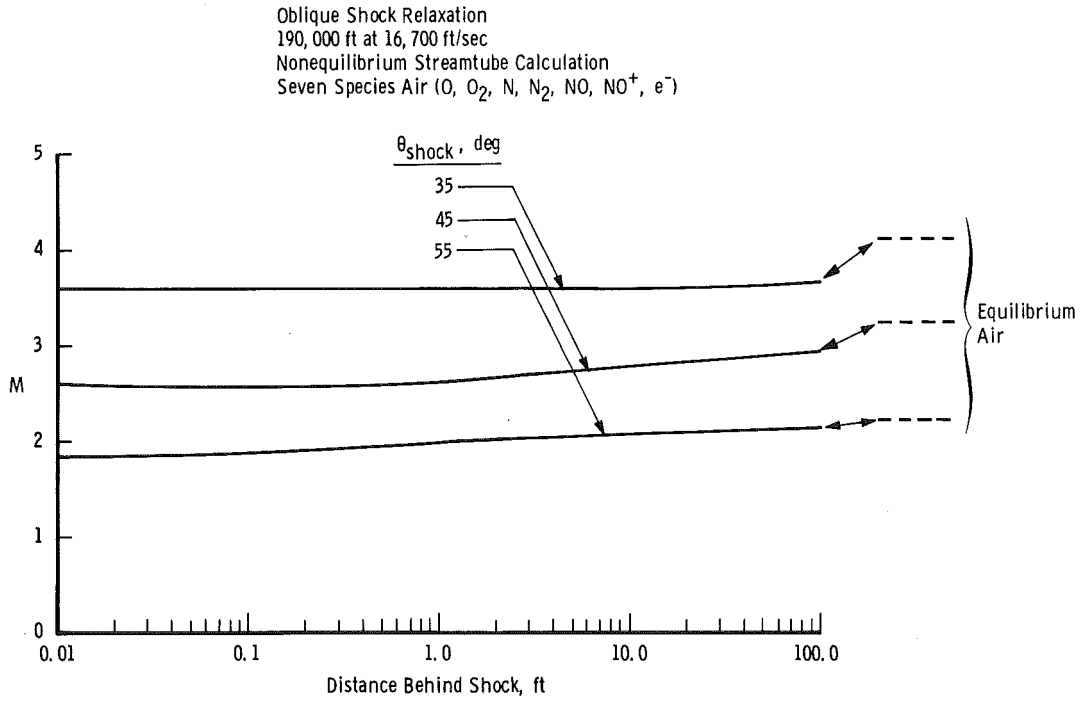

c. 190,000 ft at 16,700 ft/sec

Figure 15. Concluded.

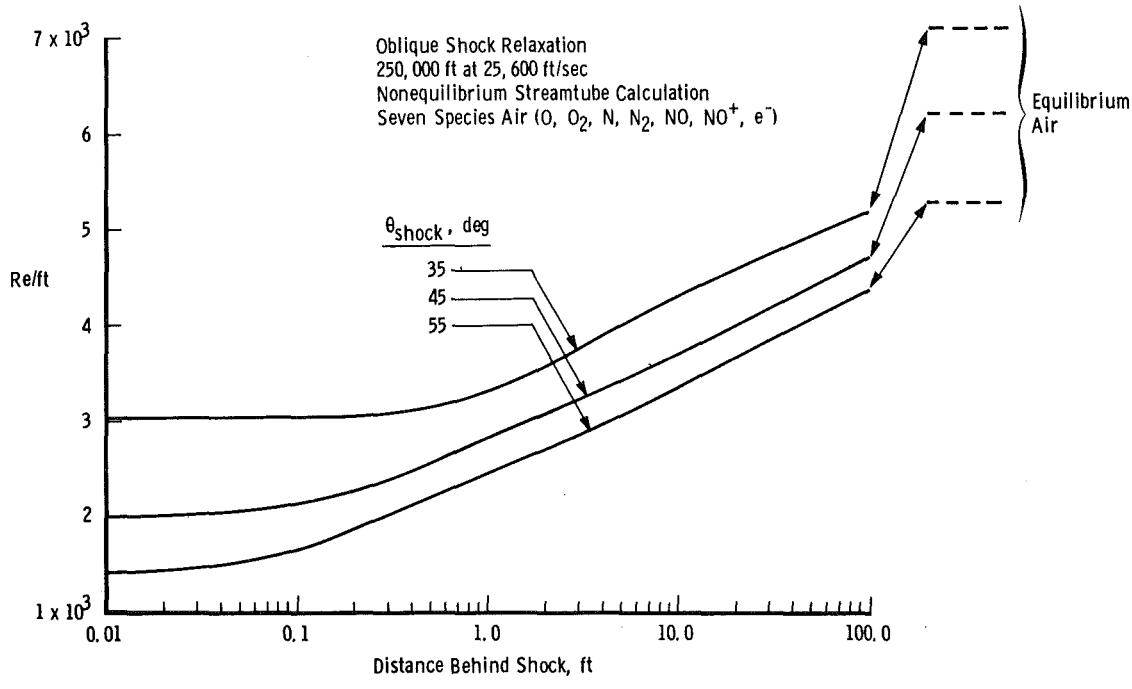

a. 250,000 ft at 25,600 ft/sec

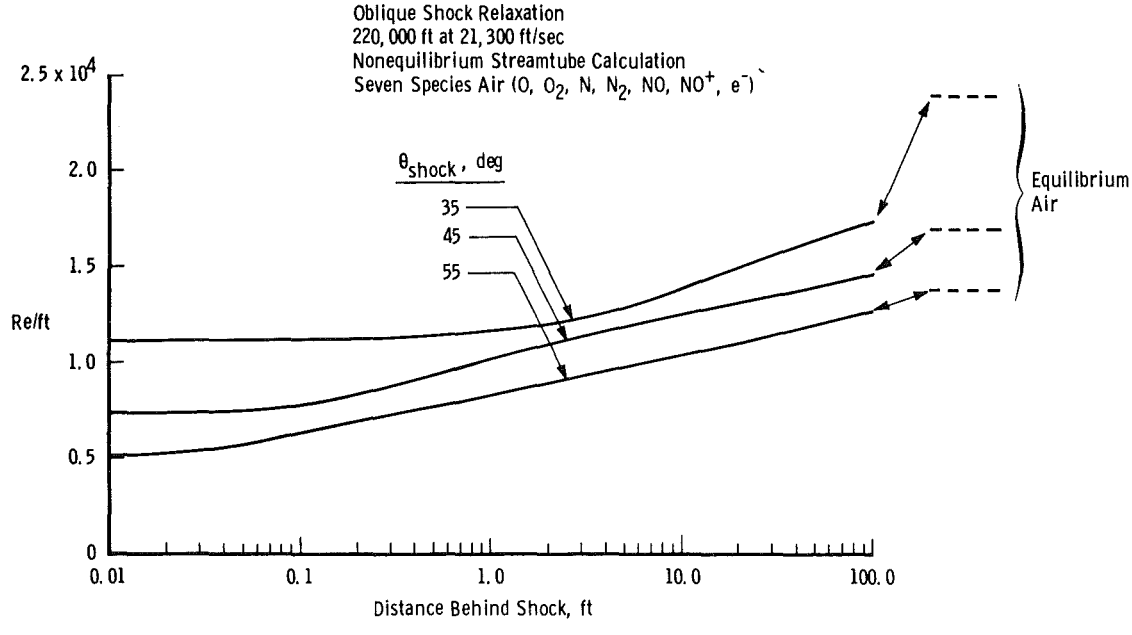

b. 220,000 ft at 21,300 ft/sec

Figure 16. Chemical nonequilibrium oblique shock relaxation effects on the local unit Reynolds number.

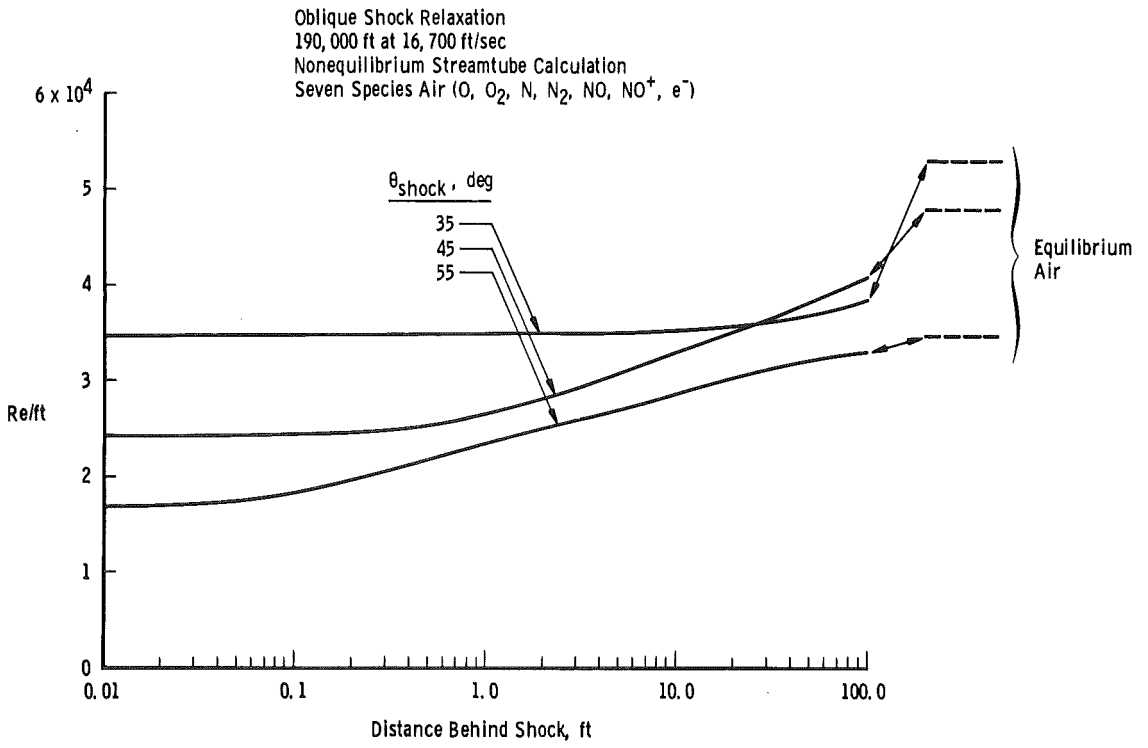

c. 190,000 ft at 16,700 ft/sec
Figure 16. Concluded.

Reynolds number is approximately 40 percent greater than the chemical nonequilibrium value at a distance of 100 ft behind the shock; this statement applies to all three altitude-velocity conditions. At the 55-deg shock angle condition, equilibrium is essentially attained at 100 ft behind the shock for the two lowest altitude conditions.

The above findings indicate that chemical nonequilibrium effects will tend to reduce both the local Mach number and local unit Reynolds number below the corresponding equilibrium air values for the same altitude-velocity and shock angle conditions. The largest chemical nonequilibrium influence is on the local unit Reynolds number at the smaller values of the shock angle. Much more detailed calculations using chemical nonequilibrium bluntbody flow-field analyses are required to fully assess nonequilibrium effects under Space Shuttle flight conditions. Until such knowledge becomes available, equilibrium air results appear, in light of the above findings, to yield reasonable estimates under flow conditions where entropy-layer swallowing is important.

8.0 IMPLICATIONS RELATIVE TO BOUNDARY-LAYER TRANSITION

The present work emphasizes the development of correlation parameters which enable hypersonic wind tunnel data to be properly scaled to flight with respect to laminar boundary-layer edge quantities under flow conditions where entropy-layer swallowing must be taken into account. The importance of these correlation parameters is directly linked to the common aerodynamic practice of correlating laminar boundary-layer transition onset in terms of local boundary-layer edge properties. One example of such a correlation, taken from Fig. 45 in Ref. 23, gives

$$Re_{e,s_t} = 0.984 \times 10^6 M_e^{0.923} \tag{13}$$

where

$$Re_{e,s_t} = (Re_e/ft)\, s_t \tag{14}$$

with s_t being the surface distance from the nose to onset of boundary-layer transition. Needless to say, accurate estimates of Re_e/ft and M_e are required in order to apply the above correlation (which is based on perfect gas hypersonic wind tunnel data for various Phase B Shuttle configurations) under real gas flight conditions where entropy-layer swallowing is important. The presently proposed correlation parameters satisfy this requirement in all respects.

The correlations developed in this investigation allow boundary-layer edge conditions and transition estimates to be determined for perfect gas wind tunnel conditions and equilibrium real gas flight conditions. The above correlation for onset of boundary-layer transition can be used in conjunction with the present oblique shock relaxation calculations to estimate the effects of chemical nonequilibrium on boundary-layer transition onset distance, s_t. Denoting chemical nonequilibrium by NEQ and chemical equilibrium by EQ, the above correlation yields the ratio

$$\frac{(s_t)_{NEQ}}{(s_t)_{EQ}} = \frac{\left(\frac{M_e^{0.923}}{Re_e/ft}\right)_{NEQ}}{\left(\frac{M_e^{0.923}}{Re_e/ft}\right)_{EQ}} \tag{15}$$

under the assumption that the correlation (which, recall, is based on perfect gas hypersonic wind tunnel results) is applicable under both chemical equilibrium and nonequilibrium conditions. Evaluating the chemical nonequilibrium parameters at a distance of 50 ft behind the shock for the altitude-velocity condition of 220,000 ft and 21,300 ft/sec yields the following:

θ_{shock}, deg	$(s_t)_{NEQ} / (s_t)_{EQ}$
35	1.30
45	1.10
55	1.04

These results indicate that, for a given altitude-velocity and shock angle condition, the effects of chemical nonequilibrium will be to increase the transition onset distance. It is to be emphasized that this finding is based on one particular transition correlation; other choices for the transition correlation may yield different trends with respect to chemical nonequilibrium effects on transition onset distance. More work is definitely needed in this area. The recent study by Lordi, Vidal, and Johnson (Ref. 24) represents one such effort similar in many respects to the present investigation.

9.0 CONCLUDING SUMMARY

The present investigation has resulted in development of correlation parameters for laminar boundary-layer edge quantities and surface heat transfer along the windward symmetry plane of the Rockwell International 139 Space Shuttle Orbiter configuration at 30 deg angle of attack. These correlation parameters enable hypersonic wind tunnel data to be properly scaled to flight under conditions where entropy-layer swallowing by the boundary layer must be considered. The proposed correlation parameters are simple to use (in an engineering sense) and accurately account for real gas (equilibrium air) effects as encountered in flight. Chemical nonequilibrium effects have been briefly examined via oblique shock relaxation in order to ascertain the validity of the equilibrium air flow-field model used in the present work. Some implications of the proposed correlation parameters on boundary-layer transition have been discussed.

REFERENCES

1. Masek, R. V. and Forney, J. A. "An Analysis of Predicted Space Shuttle Temperatures and Their Impact on Thermal Protection Systems." Paper No. 4 in NASA TM X-2272, Vol. I, April 1971, pp. 75-96.

2. Helms, V. T., III. "Evaluation of Boundary-Layer Transition Criteria for Space Shuttle Orbiter Entry." Paper No. 24 in NASA TM X-2507, Vol. II, February 1972, pp. 683-704.

3. Nagel, A. L., Fitzsimmons, H. D., and Doyle, L. B. "Analysis of Hypersonic Pressure and Heat Transfer Tests on Delta Wings with Laminar and Turbulent Boundary Layers." NASA CR-535, August 1966.

4. Patankar, S. V. and Spalding, D. B. Heat and Mass Transfer in Boundary Layers. CRC Press, Cleveland, 1968.

5. Inouye, M., Rakich, J. V., and Lomax, H. "A Description of Numerical Methods and Computer Programs for Two-Dimensional and Axisymmetric Supersonic Flow Over Blunt-Nosed and Flared Bodies." NASA TN D-2970, August 1965.

6. Aungier, R. H. "A Computational Method for Exact, Direct, and Unified Solutions for Axisymmetric Flow Over Blunt Bodies of Arbitrary Shape (Program BLUNT)." AFWL-TR-70-16, July 1970.

7. Lomax, H. and Inouye, M. "Numerical Analysis of Flow Properties About Blunt Bodies Moving at Supersonic Speeds in an Equilibrium Gas." NASA TR R-204, July 1964.

8. Levine, J. N. "Finite Difference Solution of the Laminar Boundary Layer Equations Including Second-Order Effects." AIAA Paper 68-739, presented at the AIAA Fluid and Plasma Dynamics Conference, Los Angeles, California, 1968.

9. Mayne, A. W., Jr., and Dyer, D. F. "Comparisons of Theory and Experiment for Turbulent Boundary Layers on Simple Shapes at Hypersonic Conditions." Proceedings of the 1970 Heat Transfer and Fluid Mechanics Institute. Stanford University Press, June 1970, pp. 168-188.

10. Cohen, N. B. "Correlation Formulas and Tables of Density and Some Transport Properties of Equilibrium Dissociating Air for Use in Solutions of the Boundary-Layer Equations." NASA TN D-194, February 1960.

11. Mayne, A. W., Jr., and Adams, J. C., Jr. "Streamline Swallowing by Laminar Boundary Layers in Hypersonic Flow." AEDC-TR-71-32 (AD719748), March 1971.

12. Adams, J. C., Jr. "Chemical Nonequilibrium Boundary-Layer Effects on a Simulated Space Shuttle Configuration during Re-Entry." J. Spacecraft and Rockets, Vol. 8, No. 6, June 1971, pp. 683-684.

13. Lomax, H. and Bailey, H. E. "A Critical Analysis of Various Numerical Integration Methods for Computing the Flow of a Gas in Chemical Nonequilibrium." NASA TN D-4109, August 1967.

14. Cresswell, J., Kaplan, B., Porter, R., and Sarkos, C. "Material Effects of Low Temperature Ablators on Hypersonic Wake Properties of Slender Bodies." GE TIS 67SD255, May 1967.

15. Blottner, F. G. "Non-Equilibrium Laminar Boundary Layer Flow of Ionized Air." GE TIS R64SD56, November 1964.

16. Martindale, W. R. and Carter, L. D. "Flow-Field Measurements in the Windward Surface Shock Layer of Space Shuttle Orbiter Configurations at Mach Number 8." AEDC-TR-75-5 (ADA012875), July 1975.

17. Lewis, C. H. and Burgess, E. G., III. "Altitude-Velocity Table and Charts for Imperfect Air." AEDC-TDR-64-214, January 1965.

18. Rotta, N. R. and Zakkay, V. "Effects of Nose Bluntness on the Boundary Layer Characteristics of Conical Bodies at Hypersonic Speeds." Astronautica Acta, Vol. 13, Nos. 5 and 6, 1968, pp. 507-516.

19. Ferri, A. "Some Heat Transfer Problems in Hypersonic Flow." Aeronautics and Astronautics. Pergamon Press, New York, 1960, pp. 344-377.

20. Zakkay, V. and Krause, E. "Boundary Conditions at the Outer Edge of the Boundary Layer on Blunted Conical Bodies." AIAA J., Vol. 1, No. 7, July 1963, pp. 1671-1672.

21. Rubin, I. "Shock Curvature Effect on the Outer Edge Conditions of a Laminar Boundary Layer." AIAA J., Vol. 1, No. 12, December 1963, pp. 2850-2852.

22. Vincenti, W. G. and Kruger, C. H., Jr. Introduction to Physical Gas Dynamics. John Wiley and Sons, Inc., New York, 1965.

23. Fehrman, A. L. and Masek, R. V. "Study of Uncertainties of Predicting Space Shuttle Thermal Environment." Report MDC E0639, June 1972.

24. Lordi, J. A., Vidal, R. J., and Johnson, C. B. "Chemical Nonequilibrium Effects on the Inviscid Flow in the Windward Plane of Symmetry of Two Simplified Shuttle Configurations." NASA TN D-7189, March 1973.

NOMENCLATURE

H	Total enthalpy
H_∞	Free-stream total enthalpy
h	Static enthalpy
h_e	Static enthalpy at edge of boundary layer
h_w	Wall static enthalpy
$\overline{h}$	Heat-transfer coefficient, $-\dot{q}_w/(T_{O,\infty} - T_w)$
$\overline{h}_{ref}$	Reference heat-transfer coefficient based on Fay-Riddell correlation and a scaled 1-ft spherical nose radius
L	Reference length for 139 Orbiter, 1290.3 in. full scale, 22.58 in. for 0.0175-scale model
M	Local Mach number
$M_{conical}$	Inviscid conical surface Mach number
M_e	Local Mach number at edge of boundary layer
$M_{e,NS}$	Local Mach number at outer edge of boundary layer based on isentropic expansion from the stagnation point
M_∞	Free-stream Mach number

p_o'	Free-stream pitot pressure
p_p	Local pitot pressure
p_w	Wall static pressure
$\dot{q}_w$	Wall heat-transfer rate
r	Radius as defined in Fig. 3
r_N	Nose radius as defined in Fig. 3
Re/ft	Local unit Reynolds number
Re_e/ft	Local unit Reynolds number at edge of boundary layer, $\rho_e U_e / \mu_e$
$Re_{e, NS}$	Local unit Reynolds number at edge of boundary layer based on isentropic expansion from the stagnation point
Re_{e, r_N}	Local Reynolds number at edge of boundary layer based on nose radius, $\rho_e U_e r_N / \mu_e$
$Re_{e, s'}$	Local Reynolds number at edge of boundary layer based on surface distance from sharp cone apex, $\rho_e U_e s' / \mu_e$
$Re_{e, s}$	Local Reynolds number at edge of boundary layer based on surface distance from the stagnation point, $\rho_e U_e s / \mu_e$
Re_{e, s_t}	Local Reynolds number at edge of boundary layer based on surface distance from the stagnation point to onset of boundary-layer transition, $\rho_e U_e s_t / \mu_e$
Re_∞/ft	Free-stream unit Reynolds number, $\rho_\infty U_\infty / \mu_\infty$
Re_{∞, r_N}	Free-stream Reynolds number based on nose radius, $\rho_\infty U_\infty r_N / \mu_\infty$
S	Entropy-layer-swallowing similarity parameter, $(s/r_N)/Re_{\infty, r_N}^{1/3}$
s′	Surface distance from the sharp cone apex